ABSTRACT

MECHANICAL PROPERTIES AND STRUCTURAL
STABILITY OF THE WHEAT PLANT

by Safwat Mahmoud Ali Moustafa

This study was initiated to study the behavior of the cereal grain plant under applied stresses. Since the plant stem is the principal supporter of the plant structure, the understanding of its behavior and physical properties is of major importance to the engineer. The mechanical and rheological properties of the plant stem as well as the stability of the plant structure were investigated. Tests were conducted over a period of four weeks to study the maturity effect, and were limited to three varieties of wheat--(Triticum Vulgarus)--Comanche, Redcoat and Genesee.

All tests were conducted in a testing chamber under controlled temperature and humidity conditions. Tension, compression, and bending tests were conducted to study the behavior of the straw to applied stress. Elastic and viscous properties of the straw were evaluated using elastic and viscoelastic flexure theory. The buckling stability was studied for the plant structure.

Theoretical equations were derived for the evaluation of the elastic and viscoelastic moduli from quasi-static

flexure. Critical load and deformation equations were derived from the theory of elastic stability.

The wheat plant reacted to applied forces as an elastic-plastic-viscous body. A viscoelastic model, consisting of one viscous and two simple Maxwell elements in parallel, simulated the behavior of the plant stem in compression. The stem behaved in flexure similar to two simple Maxwell elements in parallel.

The stability of the plant structure was explained by employing the theory of elastic stability together with the concepts of inelastic buckling. The existence of the nodes provided a localized increase in the inertia of the straw which contributed to the stability of the plant. The decrease in the outside diameter of the plant stem toward the plant top was assumed linear and the wall thickness constant. This cross-sectional change reduced the buckling strength of the plant by a factor which is a function of the rate of change in the cross section. The top internode, which is the longest, was the least stable. Wind force acting on the plant, as it stands in the field, was approximated by a linearly distributed horizontal force having its largest magnitude at the top of the plant. These forces greatly influenced the deformation of the plant.

As the plant reached the harvesting stage, the viscous properties decreased and the elastic properties dominated the behavior of the plant for small deformations. In this stage the head weight becomes the principal axial force acting on the plant. A high velocity wind will force the plant to deform from its initial straight shape. The strains in the top internode may exceed the elastic range. As the wind stops the plant tends to recover its original shape but retains a slightly curved shape due to the residual plastic strains in the fibers where the elastic limit was exceeded. Successive wind forces together with the growth of the plant head increase the residual plastic strain which results in the familiar bent shape of the top internode during the harvesting season. An exceptionally high intensity wind, in this stage, may result in the failure or lodging of the plant.

Approved B A Stout
Major Professor

Approved Carl W. Hall
Department Chairman

MECHANICAL PROPERTIES AND STRUCTURAL STABILITY OF THE WHEAT PLANT

By

Safwat Mahmoud Ali Moustafa

A THESIS

Submitted to
Michigan State University
in partial fulfillment of the requirements
for the degree of

DOCTOR OF PHILOSOPHY

Department of Agricultural Engineering

1966

ACKNOWLEDGMENTS

The guidance and leadership of Dr. B. A. Stout (Agricultural Engineering) is gratefully acknowledged. The inspiration provided throughout this portion of my graduate program and during the course of this investigation has made it a pleasing and rewarding experience.

Sincere appreciation is extended to Dr. W. A. Bradley (Metallurgy, Mechanics and Material Science) for his valuable suggestions and active professional interest in this study.

Additional acknowledgment is offered Dr. M. L. Esmay (Agricultural Engineering) and Dr. E. H. Everson (Crop Science) for serving as guidance committee members and providing advice and help whenever needed.

The unfailing support and encouragement provided by my wife, Samraa, has supplied inspiration needed throughout my graduate education.

To

Samraa, Mona, and Shereef

Mr. and Mrs. M. A. Moustafa

The United Arab Republic

TABLE OF CONTENTS

CHAPTER Page

LIST OF TABLES

LIST OF FIGURES

Figure		Page

Figure		Page

1. INTRODUCTION

Cereal grains are the greatest source of food on our planet. In the U. S. A. and other highly mechanized areas of the world, these crops are harvested with combines. Although these harvesters have great capacities and are very effective, they are expensive and have high power requirements.

Many researchers have sought methods of improving the efficiency and lowering the power requirements of combines. The cone thresher and the standing harvester studies at Michigan State University are recent examples.

So far, all the threshing mechanisms, either the conventional rotating cylinder or the centrifugal thresher, are based on the application of an impulsive force, either impact or the combined effect of impact and acceleration forces, until the grains are separated from the plant head.

Successful mechanical harvesting depends both on technical factors and on the extent to which the plant's agrotechnical and morphobiological properties are suited for mechanized harvesting. The physical properties of most agricultural materials which influence the machine design or operation and the quality of the final product are not completely understood. Increased knowledge of the physical properties of the cereal grain plant will be of value not only to engineers but also to plant scientists and breeders who are concerned about the lodging problems in these plants. Hence, one must consider the physico-mechanical properties of the plants not only when designing new machinery, but also when breeding new varieties and perfecting methods for their cultivation.

The design of farm machinery started as an art. However, with the tremendous progress in technology of the last fifty years it became essential for the agricultural engineer to know and understand in detail the fundamental anatomical and mechanical characteristics of the biological materials with which he is dealing, and to have this information in his engineering language. Although the engineer has collected most of the basic information about the behavior of engineering materials, he has not yet collected the needed data on materials of biological origin. One basic reason for that is the heterogeneity and complexity of their structure.

Mechanical properties of a material have been defined as the properties that determine the behavior of the material under applied forces and loads. One of the most widely used and most easily interpreted methods of specifying the behavior of materials is in terms of mechanical models. A mechanical model normally consists of an element or a combination of elements whose characteristics and behavior under applied forces are known.

Objective

The general objective of this study was to investigate the basic physical and mechanical properties of the wheat plant and express them in engineering terms. Specific objectives were to:

1. Develop a theoretical model for the wheat plant, as a whole, for the study of its stability and strength.
2. Develop a viscoelastic model for wheat straw that represents its behavior under applied stresses.
3. Verify the validity of the theoretical models of the plant by experimental evaluation of plant parameters.
4. Determine the effect of maturity on the various plant parameters.

2. REVIEW OF LITERATURE

2.1 Physical Structure of Biological Materials

The cell is the smallest structural unit of a biological material. The plant cell is composed of a non-protoplasmic rigid wall and an inner cytoplasmic fluid. The cell wall, being the supporter of the cell, determines its shape and texture. The plant has two types of walls, a primary wall and a secondary wall. Living cells, which carry out life processes, have only a primary wall whereas non-living supportive cells have an additional secondary wall.

Primary walls are composed of a fine mesh network of cellulose fibrils which are filled with pectic and hydrophilic compounds. The secondary walls are composed of crystalline cellulose grouped into coarse branching strands which are encrusted with pectins, hemicelluloses and lignins. Frey-Wyssling (1952) reported that primary walls were capable of up to 50 percent extension as compared with about two percent for secondary walls. This is due to the large amount of amorphous cellulose and pectic compounds in primary walls as contrasted to crystalline cellulose and lignins in secondary walls.

Kollman (1964) reported that the woody cell wall consists of 45-65 percent cellulose, which is formed from glucose anhydrides. He also reported that x-ray optical studies have shown four cellobios residues form the crystalline element body of cellulose. Increasing crystallinity has a very strong influence on the most important physical and mechanical properties of cellulose containing fiber. With it the density, the modulus of elasticity, and the tensile strength increase, while the moisture absorption, the swelling and stretchability decrease.

Such mechanical properties as of cellulose-containing fibers and tissues may depend, besides crystallinity, on the orientation of the crystalline regions of the fiber axis.

Kollman (1964) also reported that the crystallized parts of the cell wall behave as elastic elements while amorphous regions are like viscous elements.

Generally the cell wall behaves in what is believed to be a nearly elastic manner while the cellular fluids are liquids exhibiting a viscous behavior. Therefore, it seems logical to represent the mechanical behavior of selected biological materials by using mechanical models composed of elastic and viscous elements.

2.2 Physical Structure of the Grain Crop Plant

The wheat plant consists of three major parts. The root, the stem, and the head. The root functions are to support the plant in the soil, to gather water and minerals from the soil, and transport them to the stem of the plant. The stem represents the major part of the plant structure above the ground. It supports the head and leaves of the plant and carries out life processes. The head grows at the top of the plant and carries the grain.

The plant stem varies in height between two to six feet. The stem can be approximated by a hollow tube with a gradually decreasing diameter toward the plant top. The stem has a number of nodes ranging between four and five. The distance between nodes (internode) increases toward the plant top.

The node represents the origin of the leaf. In the nodal area, the stem slightly decreases in diameter and the wall becomes thicker until it becomes solid at the connection with the base of the leaf.

All elements entering into the composition of the plant stem--the strongest, as well as the weak pith--play more or less important parts in the plant's resistance to the action of external forces (Esau, 1965).

Burmistrova (1956) reported that the plant stem was considered as a tubular columnar structure with a height to diameter ratio of four to six times greater than that of architectural structures.

Percival (1921) reported that in the stem of the wheat plant the course of vascular bundles through the internode and the leaf sheath is practically parallel.

Near the node the leaf sheath is considerably thickened, attaining its maximum thickness just above its union with the stem. The stem, on the other hand, decreases in thickness in the same direction and has the smallest diameter above the junction with the leaf sheath. Below the junction of leaf sheath and stem, the smaller of the leaf traces are prolonged in the peripheral part of the axis. The larger leaf traces become part of the inner cylinder of the strands. The bundles of the internode located above the leaf insertion assume a horizontal and oblique course and are reoriented toward a more peripheral position in and below the node.

2.3 Physical and Mechanical Properties

Agricultural materials, being composed of structural substances and fluids, do not react in a purely elastic manner. Rather their response is a combination of elastic, plastic and viscous behavior.

A number of investigators have studied the mechanical behavior of agricultural materials by treating them as engineering materials. Suggs and Splinter (1964) studied the behavior of tobacco stalks in bending. They found a difference between compression and tension moduli. They also observed a viscoelastic effect as exhibited in the stress relaxation behavior of the stalks. This effect was predominant at low strain rates.

Halyk and Hurlbut (1964) applied engineering material testing procedures to alfalfa stems in order to determine their ultimate tensile and shear strength.

McClelland and Spielrin (1957) reported the existence of a precise relationship between the force required to cause failure in bending and linear density of the plant material for three pasture plants--Wimmera ryegrass (*Lolium rigidum*), lucerne (*Medicago sativa*), and Algerian oats (*Avena byzantina*).

The Soviet All-Union Scientific Research Institute for Agricultural Machine Building (VISKHOM) built in 1934 a special laboratory to specialize in investigations on the physicomechanical properties of grain crops, rice, corn, sunflower, potato, sugar beet, various fodder crops, flax, hemp, castor, soyabean, groundnuts, tobacco, etc. Burmistrova, *et al*. (1956) reported some of their data on size, weight, volume and quantitative properties of plants, and strength indexes of various plant's parts subjected to the action of different machine working parts. Other results obtained from these investigations were on friction coefficients of various plants subjected to different surface conditions, speeds, pressures, etc. These investigations were for the purpose of providing experimental basis for the machine designer's work.

Diener (1965) used static and dynamic loading to study the mechanical properties of cherry bark and wood. He determined the maximum strength of bark specimens from tensile loading. He also measured the elastic and viscous properties of bark and green wood specimens using the elastic and viscoelastic flexure theory. He derived an approximate and an exact equation for determining the viscoelastic modulus from dynamic flexure. He concluded that the strength of bark was highly dependent on the direction of the applied force, i.e., the material is anisotropic.

The use of mechanical models to approximate the behavior of materials of biological origin has been proven to be useful. Most mechanical models consist of an element or number of mechanical elements whose behavior under applied stresses is known. This provided the possibility of describing and explaining a wide range of behavior.

Zoerb (1958) studied the mechanical and rheological properties of cereal grains. He obtained stress-strain curves for both the whole kernel and a core specimen made by cutting off each end. Information derived from these studies was used for the evaluation of hysteresis losses, moduli of resilience, and moduli of elasticity. He also conducted stress relaxation studies on pea beans using varying loading rates. The relaxation data was fitted to a two-element Maxwell model which gave a close approximation of the observed behavior.

Mohsenin, et al. (1963) proposed a qualitative model to represent the viscoelastic nature of creep behavior for fruits in terms of the analogous behavior of a Maxwell model in series with a Kelvin-Voigt model.

Finney, et al. (1963) considered the potato tuber as a linear viscoelastic body and established a physical basis for this consideration by studying the constitutive components of the potato tuber. They also studied the stress relaxation properties of the tubers when axially loaded between parallel plates. The relaxation was represented qualitatively by the equivalent response of four Maxwell models in parallel. Timbers (1964) studied both creep and stress relaxation behavior of Netted gem Potato. He also proposed a mechanical model to represent the tuber behavior.

Shpolyanskaya (1952) studied the structural-mechanical properties of wheat kernels. She reported that wheat kernels behaved as an elastic-plastic-viscous body which exhibited creep, stress relaxation, and elastic aftereffects. She proposed a mechanical model to represent the time-dependent behavior of a grain subjected to uniaxial compression. She also utilized the classical Hertz solution for contact stresses to evaluate the modulus of deformability for the grain.

Morrow (1965) studied the viscoelastic properties of McIntosh apples subjected to both uniaxial and bulk compression. Mechanical models were chosen to represent both creep and relaxation behavior.

Morrow and Mohsenin (1965) proposed standardization of techniques for the evaluation of mechanical properties of agricultural products. They suggested that all mechanical properties should be evaluated in terms of common engineering parameters as a first approximation. They also suggested that all moduli of compliances should be fitted to viscoelastic models for the purpose of obtaining meaningful time constants and other viscoelastic parameters. They obtained a consistent correlation between experimental responses of McIntosh apples and those predicted by viscoelastic models.

3. THEORETICAL CONSIDERATIONS

3.1 Mechanical Properties

Mechanical properties are the properties that determine the behavior of the material under applied forces. Those properties which are concerned with flow and deformations are referred to as rheological properties. Rheology, generally, considers those stress strain relationships of the materials which are time dependent.

Jastrzebski (1964) reported that all load-carrying materials can be divided into three main divisions according to the mechanism involved in their deformation under applied forces. These are elastoplastic, viscoelastic, and elastic materials. It follows that three basic types of deformations are involved in the response of all engineering materials to applied forces. These are elastic, plastic, and viscous deformations.

3.1a Elasticity

A material is called elastic when the deformation produced in the body is wholly recovered after removal of the forces. For linearly elastic materials, the relation between stress and the corresponding strain, in the elastic range of the material, is governed by Hooke's law. Hooke's law states that the stress is proportional to strain and independent of time. It follows that the ratio of stress to strain is a constant characteristic of a material, and this proportionality constant is referred to as the modulus of elasticity.

For an isotropic material each stress will induce corresponding strain, but for an anisotropic material a single stress component may produce more than one type of strain in the material. Since there are three main types of stress--tension, compression and shear--there will be three corresponding moduli of elasticity.

Very few materials behave as perfectly elastic bodies because of structural imperfections. Many materials yield a curved stress-strain diagram practically from its beginning. The definition of the modulus of elasticity does not require the stress-strain curve to be linear. If the curve is not linear, the modulus of elasticity should be taken as a secant or tangent elastic modulus. A tangent elastic modulus is defined as an increment of stress divided by an increment of strain for an elastic substance.

3.1b Plasticity

Many materials when stressed beyond a certain minimum stress show a permanent, nonrecoverable deformation. This is called plastic deformation, and it is the result of permanent displacement of atoms, molecules, or groups of atoms and molecules from their original positions after the removal of stress.

An ideal plastic body, also called St. Venant's solid, is represented on the stress-strain diagrams as a line parallel to the strain axis at a distance corresponding to the yield stress of the material.

Closely connected with plastic deformation is the concept of plasticity, which is defined as the ability of the material to be deformed continuously and permanently without rupture during the application of a force that exceeds the yield value of the material.

Most of the materials show deviations from both perfect elastic and ideal plastic behavior; therefore, the relationship between stress and strain will not be linear. They show a slightly curved line in the elastic range and a considerable increase in stress during plastic deformation.

Jastrzebski (1964) reported that the mechanism of plastic deformation is essentially different in crystalline and amorphous materials. Crystalline materials undergo plastic deformation as the result of slip along a definite crystollographic plane, whereas in amorphous materials sliding of individual molecules or groups of molecules past one another occurs, resulting in a flow.

3.1c Viscoelasticity

The classical theory of elasticity deals with mechanical properties of perfectly elastic solids, for which, in accordance with Hooke's law, stress is assumed always directly proportional to strain but independent of the rate of strain. The theory of hydrodynamics deals with properties of perfectly viscous liquids, for which in accordance with Newton's law the stress is always directly proportional to rate of strain but independent of the strain itself. These categories are idealizations; however, as mentioned before, any real solid shows deviations from Hooke's law under suitably chosen conditions, and it is probably safe to say that any real liquid would show deviations from Newtonian flow if subjected to sufficiently precise measurements.

There are two important types of deviations. First, the strain (in a solid) or the rate of strain (in a liquid) may not be directly proportional to the stress but may depend on stress in a more complicated manner. Such stress anomalies are familiar when the elastic limit is exceeded for a solid. Second, the stress may depend on both the strain and the rate of strain together, as well as higher time derivatives of the strain. Such time anomalies evidently reflect a behavior which combines liquid and solid like characteristics, and they are therefore called viscoelastic.

Both stress and time anomalies may of course coexist. If only the latter is present, we have <u>linear</u> viscoelastic behavior; then, in a given experiment the ratio of stress to strain is a function of time alone, and not of the stress magnitude.

When a material exhibits linear viscoelastic behavior, its mechanical properties can be duplicated by a model consisting of some suitable combination of springs, which obey Hooke's law, and viscous dashpots (pistons moving in oil), which obey Newton's law.

To simulate a real material, the model may require an infinite number of units with different spring constants and flow constants, but if each unit is linear (Hookean or Newtonian respectively) the overall behavior is linear.

In general viscoelastic materials may include as special cases, the ideal elastic (Hookean) solid at one extreme and the ideal viscous (Newtonian) fluid at the other. All other viscoelastic materials may therefore be viewed as incorporating in varying amounts through suitable combinations of the characteristic behavior associated with those two materials. Accordingly, simple models composed of suitable arrangements of linear springs (Hookean elements) and viscous dashpots (Newtonian elements) serve well to portray the phenomenological behavior of viscoelastic media.

A viscoelastic model (Figure 3.1) is composed of two (or more) primary elements, the elastic element and the viscous element.

(i) The elastic element (Hookean): or spring element:

$F = Eu$; where: E = spring modulus = const.

u = displacement

(ii) The viscous element (Newtonian): or dashpot element:

$F = \eta \frac{du}{dt} = \eta Du$; where: η = the viscosity of the dashpot fluid

$D = \frac{d}{dt}$

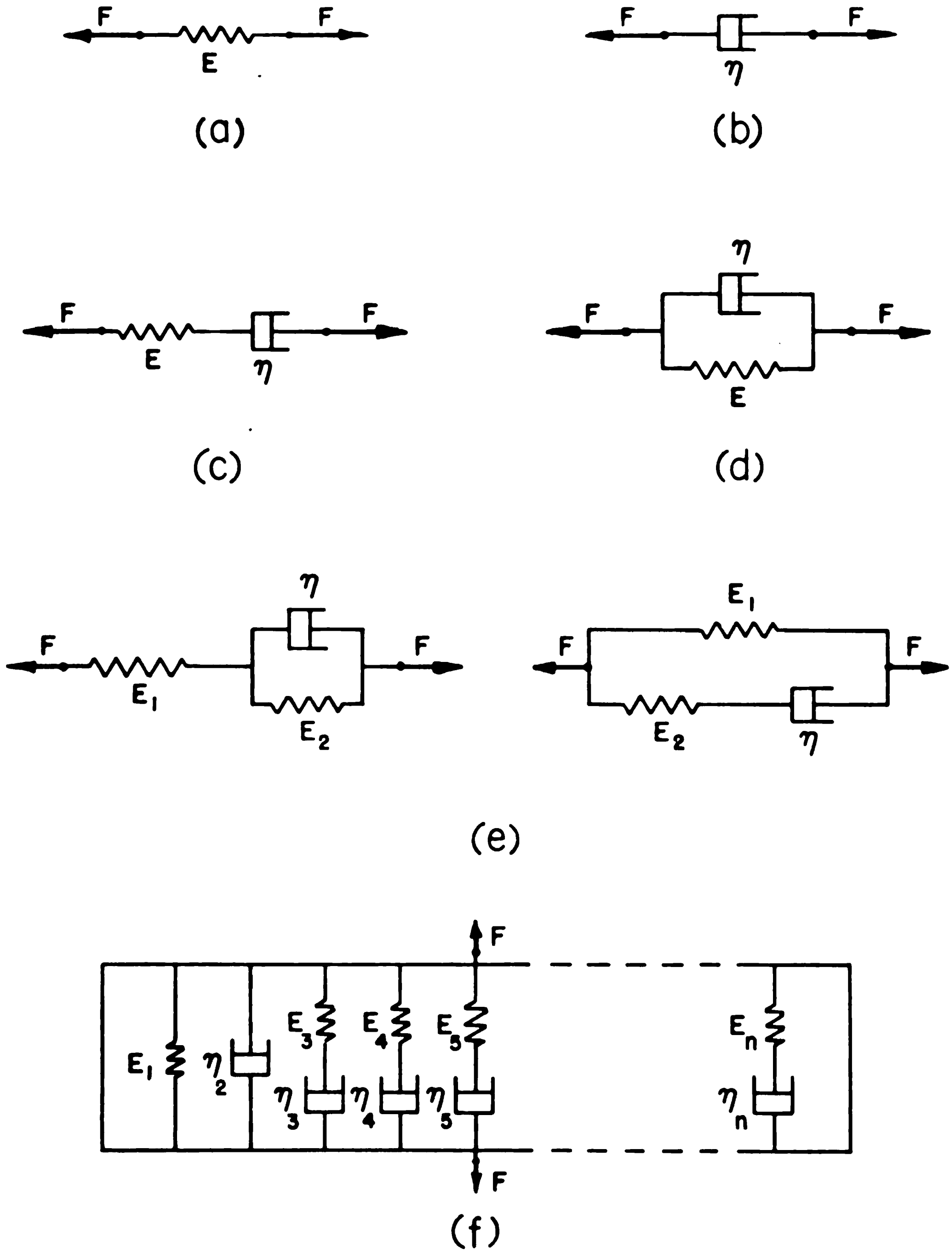

Figure 3.1--Viscoelastic models: (a) Elastic element (Hookean),(b) Viscous element (Newtonian), (c) Maxwell model, (d) Kelvin-Viogt model, (e) Three element model, (f) Generalized Maxwell model.

(iii) Combination in series: (Maxwell model):

$Du = (\frac{1}{E})\ DF + (\frac{1}{\eta})\ F.$

(iv) Combination in parallel: (Kelvin-Voigt model):

$F = Eu + \eta\ Du.$

(v) Generalized Maxwell Model:

A parallel combination of a Hookean element, Newtonian element, and a large number of Maxwell models.

I. If this model is given a <u>sudden deformation</u> (u) defined as $u = K\ H(t)$, where $H(t)$ is the Heaviside unit function, defined by

$H(t) = 0,\ t < 0$

$H(t) = 1,\ t \geq 0$

(e.g., a constant strain situation), the problem of stress relaxation can be represented in terms of the mathematical equation

$$F(t) = K\ E_1\ H(t) + K\eta_2\ \delta(t)$$

$$+ K \sum_{i=3}^{n} E_i(e^{-E_i t/\eta_i})\ H(t)$$

where $\delta(t)$ = the Dirac delta function = $D\ H(t)$

The force response to a unit extension $u(t) = H(t)$, and excluding the constant and delta components, is defined by Bland (1960) as the "relaxation function," denoted by $X(t)$. For the generalized Maxwell model, therefore, it is:

$$X(t) = \sum_{i=3}^{n} E_i \, (e^{-E_i t/\eta_i}) \, H(t)$$

$$= \sum_{i=3}^{n} E_i \, (e^{-t/\tau_i}) \, H(t)$$

where:

$\tau_i = \frac{\eta_i}{E_i}$ = the relaxation time

II. Similarly for a constant strain rate loading (R)

$$F(t) = E_1 \int R dt + R\eta_2$$

$$+ \sum_{i=3}^{n} E_i \, R\tau_i \, (1 - e^{-t/\tau_i}) \qquad (3.1)$$

Generalized Maxwell models having various number of Maxwell models in parallel can be used to represent the stress relaxation in materials. If the stress falls to zero for large values of time then there should be no spring in parallel with the other elements when a model is used to simulate the behavior of this material. Likewise, if there is an indication that it responds as a rigid body for increasingly high rates of deformation, then there should be a dashpot in parallel with the other elements of the Maxwell model.

After a satisfactory model is postulated, the relaxation function, and the complete viscoelastic behavior of the material under various types of loading can be mathematically defined.

This general discussion of various types of behavior should help in the understanding and analysis of the behavior of the wheat plant. Because of the existence of both the viscous and elastic-like properties in the plant cell, one would expect to have a behavior that combined more than one of the idealized conditions discussed previously.

The first part of this study deals with the behavior under applied loads, as well as the influence of the time factor. Once this is understood, it will then be possible to proceed in the second part of the study which deals with the structural stability of the plant.

3.2 The Theory of Elastic Stability

Consider an element of a beam subjected to longitudinal and transverse loads as shown in Figure 3.2. The differential equation of the displacement in the y-direction takes the form

$$\frac{d^2}{dx^2}\left(EI\,\frac{d^2y}{dx^2}\right) + \frac{d}{dx}\left(P\,\frac{dy}{dx}\right) = q, \qquad (3.2)$$

where: P = axial compressive load

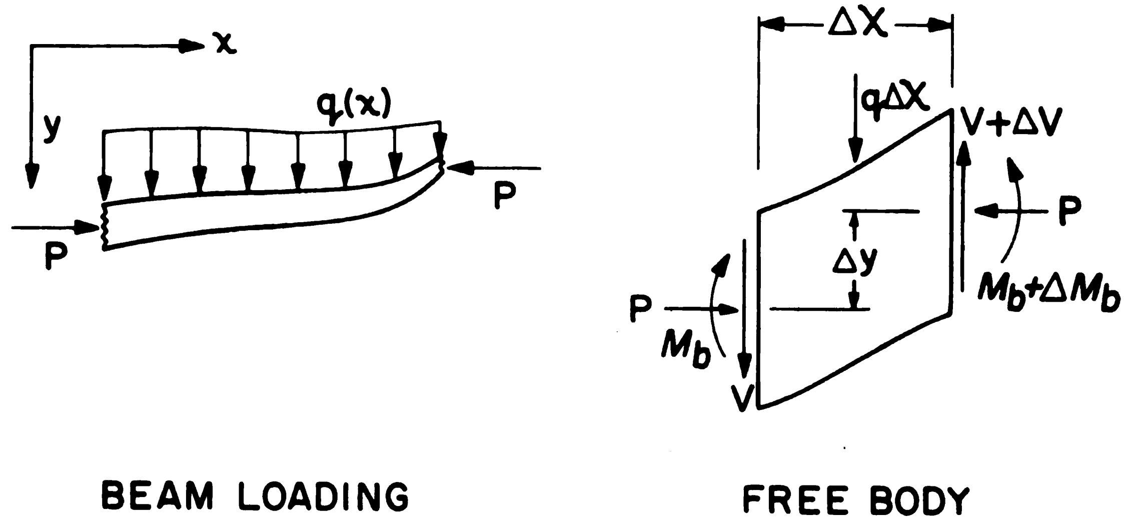

Figure 3.2--An element of elastic beam showing loading condition and forces on a free body.

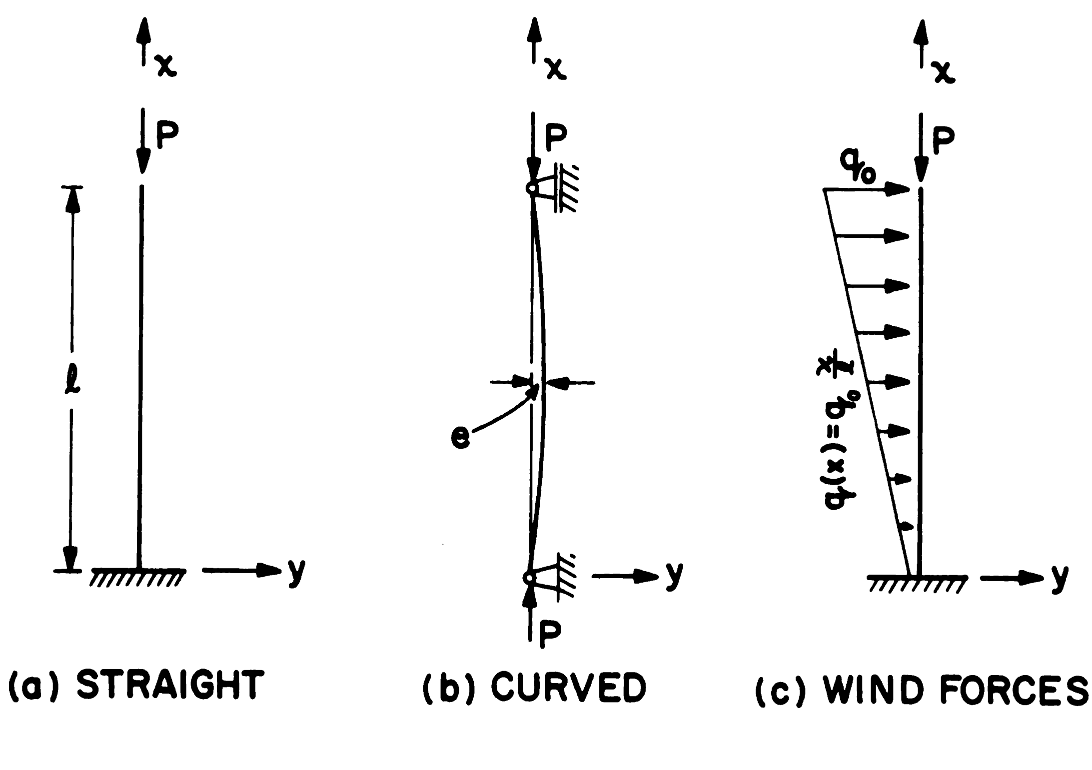

Figure 3.3--Elastic columns under different loading conditions.

EI = flexural stiffness of the section

q = transverse load per unit length.

3.2a Straight Column

Consider a flexible straight column fixed at one end and free at the other, and subjected to an axial load P (Figure 3.3a). Assume that EI, the bending stiffness, is uniform, q = 0, i.e., no transverse load, and that the buckling occurs in the x-y plane. Under these conditions the governing equation 3.2 will be reduced to the form

$$\frac{d^4y}{dx^4} + \frac{P}{EI}\frac{d^2y}{dx^2} = 0 \qquad (3.3)$$

with the boundary conditions:

$$\left.\begin{aligned} y &= 0 \\ \frac{dy}{dx} &= 0 \end{aligned}\right\} \text{ at } x = 0,$$

and

$$\left.\begin{aligned} M_b &= -\,EI\frac{d^2y}{dx^2} = 0 \\ V &= EI\frac{d^3y}{dx^3} + P\frac{dy}{dx} = 0 \end{aligned}\right\} \text{ at } x = L.$$

A possible solution of equation 3.3 takes the form

$$y = c_1 + c_2x + c_3 \sin\sqrt{\frac{P}{EI}}\,x + c_4 \cos\sqrt{\frac{P}{EI}}\,x, \qquad (3.4)$$

and considering the given boundary conditions, the expression for the deflection curve takes the form

$$y = c_1 \left[1 - \cos \left(\frac{2n-1}{2}\right) \frac{\pi x}{L}\right], \text{ for } n = 1,2,3,\ldots$$

from which the value of P, for the first mode of buckling, is

$$P \text{ (the critical load)} = \frac{\pi^2 EI}{4L^2} \tag{3.5}$$

also the corresponding deflection curve is

$$y = c_1 \left(1 - \cos \frac{\pi x}{2L}\right) \tag{3.6}$$

Similarly if the column was considered to be hinged from both ends, the corresponding critical load, for the first mode of buckling, will be

$$P_{critical} = \frac{\pi^2 EI}{L^2} \tag{3.7}$$

3.2b <u>Initial Curvature</u>

When a bar is submitted to the action of the lateral load only, a small initial curvature of the bar has no effect on the bending, and the final deflection curve is obtained by superposing the ordinates due to initial curvature on the deflection calculated as for a straight bar. However, if there is an axial force acting on the bar, the deflection produced by this force will be substantially influenced by the initial curvature.

Consider the initial shape of the column axis to be given by the equation

$$y_o = e \sin \frac{\pi x}{L} \tag{3.8}$$

i.e., it initially has the form of a sine curve with maximum ordinate at the middle equal to e, and under the action of the longitudinal compressive force P (Figure 3.3b). Additional deflection, y_1, will be produced so that the final ordinates of the deflection curve are

$$y = y_o + y_1 \tag{3.9}$$

The bending moment at any cross section is

$$M = P\,(y_o + y_1)$$

also $$M = -\,EI\,\frac{d^2y_1}{dx^2}$$

or $$\frac{d^2y_1}{dx^2} = -\,\frac{P}{EI}\,(y_o + y_1)$$

therefore $$\frac{d^2y_1}{dx^2} + k^2y_1 = -k^2e \sin \frac{\pi x}{L} \tag{3.10}$$

where $$k^2 = \frac{P}{EI}$$

The general solution of equation 3.10 is

$$y_1 = A \sin kx + B \cos k x + \frac{e}{\frac{\pi^2}{k^2 L^2} - 1} \sin \frac{\pi x}{L} \qquad (3.11)$$

From the boundary conditions.

$$y_1 = 0, \text{ for } x = 0 \text{ and } x = L,$$

$$A = B = 0.$$

Introducing the notation

$$\alpha = \frac{P}{P_{cr}} = \frac{P}{\frac{\pi^2 EI}{L^2}} = \frac{PL^2}{\pi^2 EI} = \frac{k^2 L^2}{\pi^2},$$

then $$y_1 = \frac{\alpha}{1 + \alpha} e \sin \frac{\pi x}{L},$$

and the final ordinates of the deflection curve are

$$y = y_o + y_1 = e \sin \frac{\pi x}{L} \left(1 + \frac{\alpha}{1 - \alpha}\right)$$

$$= \frac{e}{1 - \alpha} \sin \frac{\pi x}{L} \qquad (3.12)$$

This equation shows that the initial deflection, e, at the middle of the column is magnified in the ratio $\frac{1}{1 - \alpha}$ by the action of the longitudinal compressive force. When the longitudinal compressive force, P, approaches its critical value, and α approaches unity, the deflection ordinate, y, increases indefinitely.

3.2c <u>Influence of the Lateral Forces</u>

The wind forces acting on the plant in the field can be approximated by a linearly distributed lateral force having its largest value at the plant head.

Consider a straight column subject to longitudinal force P together with a linearly distributed force $q(x) = q_o \frac{x}{L}$, (Figure 3.3c). Assuming P and EI to be constant, equation 3.1 becomes

$$EI \frac{d^4y}{dx^4} + P \frac{d^2y}{dx^2} = - q_o \frac{x}{L} ,$$

or

$$\frac{d^4y}{dx^4} + k \frac{d^2y}{dx^2} = - \frac{q_o x}{EIL} , \qquad (3.13)$$

where

$$k^2 = \frac{P}{EI} .$$

The general solution of equation 3.13 takes the form

$$y = A \sin k x + B \cos k x + C x + D - \frac{q_o x^3}{6\ PL} , \qquad (3.14)$$

and A, B, C, D are constants of integration that must be evaluated from the boundary conditions:

$$\left. \begin{aligned} y &= 0, \\ \frac{dy}{dx} &= 0 \end{aligned} \right\} \text{ at } x = 0$$

$$\left.\begin{aligned} &\text{and} \quad \frac{d^2y}{dx^2} = 0 \\ &\frac{d^3y}{dx^3} + k^2 \frac{dy}{dx} = 0 \end{aligned}\right\} \text{ at } x = L.$$

These conditions together with equation 3.14 yield the following values for the integration constants

$$A = -\frac{C}{k} = -\frac{q_o}{Pk}\left(\frac{1}{k^2 L} + \frac{L}{2}\right)$$

and

$$B = -D = -\frac{q_o}{P\,k^2 \cos kL}\left[1 - \left(\frac{1}{kL} + \frac{kL}{2}\right)\sin kL\right]$$

Substituting these values of the constants in equation 3.14 yields

$$y = \frac{q_o}{Pk}\left(\frac{1}{k^2} + \frac{L}{2}\right)(kx - \sin kx)$$

$$+ \frac{q_o}{Pk^2 \cos kL}\left[1 - \left(\frac{1}{kL} + \frac{kL}{2}\right)\sin kL\right][1 - \cos kx]$$

$$- \frac{q_o x^3}{6\,PL} \qquad (3.15)$$

In this equation it is clear that the deformation is greatly influenced by the lateral forces. This situation is similar to the one discussed in section 3.2b in the sense that deformation takes place before the critical load is reached.

3.2d Variation of the Moment of Inertia

Many researchers treated the stability problem of built-up columns of varying stiffness. Bleich (1951) presented the solutions for columns with variable sections. This available information may be utilized to study the influence of the change in the dimensions of the plant stem cross section on its stability. As the plant stands in the field, the stem cross section has its largest dimensions just above the soil, and gets smaller toward the top of the plant until it reaches its smallest dimension just below the plant head.

Under the assumption that this cross-sectional variation is gradual, the whole plant may be considered analogous to half of a column hinged from both ends, changing in cross section symmetrically about its midpoint and with straight cords as shown in Figure 3.4a.

For experimental purpose, a specimen of varying cross section was hinged from both ends and tested for stability. This case could be considered analogous to that of a non-symmetrical column changing in cross section with straight chords as shown in Figure 3.4b.

Case (i): Symmetrical Column with Straight Chords Fig. 3.4a.

Denoting by I_m the moment of inertia at midpoint and by I_x its value at the reference point x, one may write

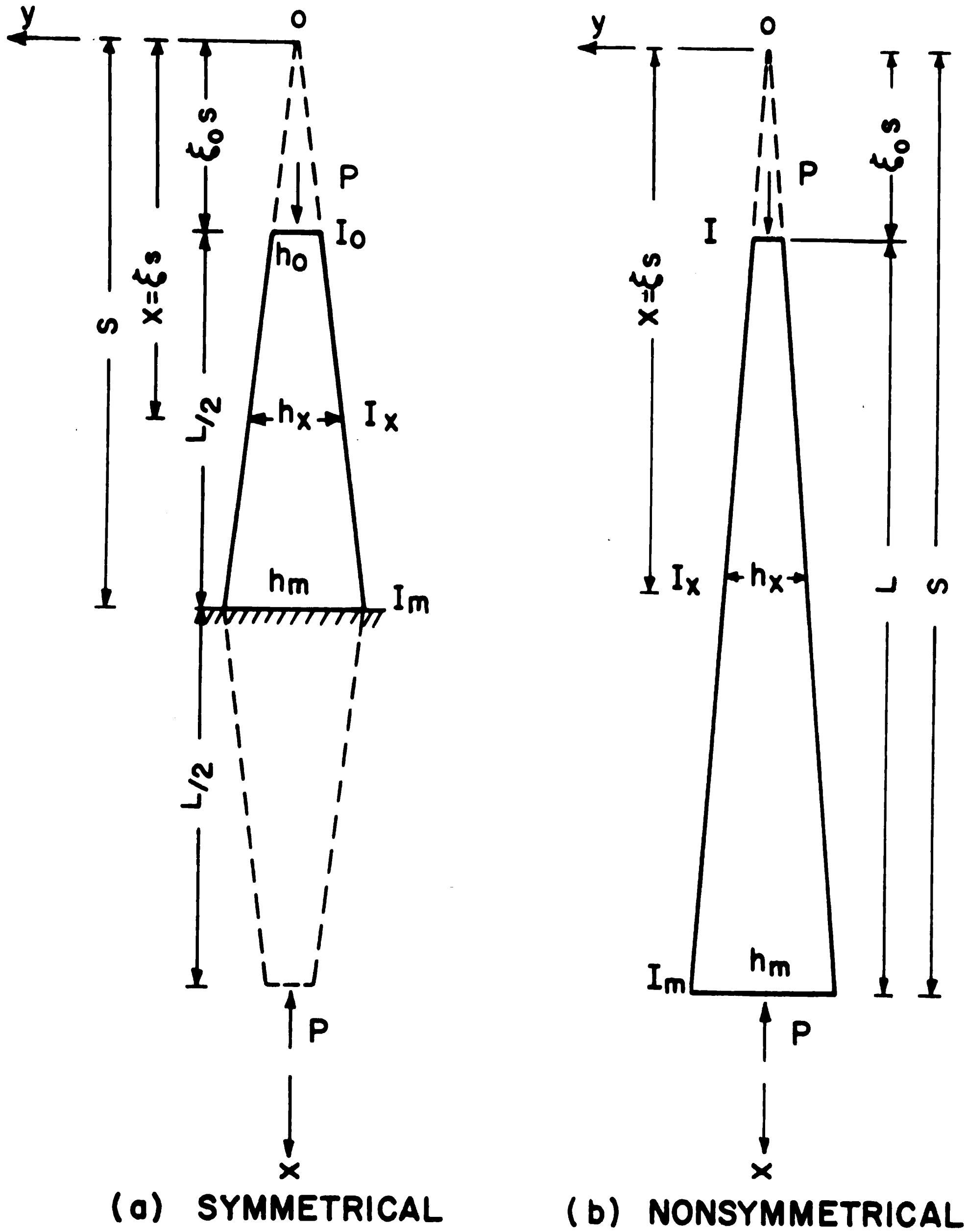

Figure 3.4--Columns with varying cross sections.

$$I_x = I_m \frac{h^2_x}{h^2_m} = I_m \frac{x^2}{s^2} = I_m \xi^2 \qquad (3.16)$$

where $\xi = \frac{x}{s}$ is a dimensionless quantity.

The bending moment is

$$M = P y = - E_t I_x \frac{d^2y}{dx^2}$$

or

$$E_t I_x \frac{d^2y}{dx^2} + P y = 0. \qquad (3.17)$$

Substituting I_x from equation 3.16 and introducing

$$\alpha^2 = \frac{P s^2}{E_t I_m}$$

leads to the differential equation with variable coefficients

$$\xi^2 \frac{d^2y}{d\xi^2} + \alpha^2 y = 0 \quad . \qquad (3.18)$$

The general solution of this equation is

$$y = \sqrt{\xi} [A_1 \sin (K \log_e \xi) + A_2 \cos (K \log_e \xi)], \quad (3.19)$$

where $K = \sqrt{\alpha^2 - \frac{1}{4}}$; and A_1 and A_2 are integration constants. Substituting equation 3.19 into the boundary conditions:

$$y = o \quad \text{at } \xi = \xi_o = \frac{h_o}{h_m},$$

and $$\frac{dy}{d\xi} = o \quad \text{at } \xi = 1,$$

results in the equations

$$A_1 \sin\left(K \log_e \frac{h_o}{h_m}\right) + A_2 \cos\left(K \log_e \frac{h_o}{h_m}\right) = 0,$$

and $$A_1\ K + \frac{A_2}{2} = 0.$$

The non-trivial solutions exist only if the determinant condition

$$\tan\left(K \log_e \frac{h_o}{h_m}\right) - 2\ K = 0$$

which has an infinite number of roots K. The smallest root K_1 defines the critical load, P_{cr}, as follows

$$P_{cr} = \frac{E_t\ I_m}{4a^2}\ (1 + 4\ K_1{}^2)$$

which can be written as

$$P_{cr} = \mu \frac{\pi^2 E_t\ I_m}{L^2} \tag{3.20}$$

where the factor μ is defined by

$$\mu = \frac{1 + 4\ K_1{}^2}{4\pi^2} \left(\frac{L}{s}\right)^2 = \frac{1 + 4\ K_1^2}{\pi^2} \left(1 - \frac{h_o}{h_m}\right)^2. \tag{3.21}$$

Equation 3.20 indicates that the critical load, P_{cr}, is found as the critical load of a column with a constant cross section having an equivalent moment of inertia $I = \mu I_m$, where μ is given by equation 3.21.

Case (ii): Nonsymmetrical Column with Straight Chords Figure 3.4b.

In this case equation 3.19 is applied to the boundary conditions:

$$y = 0 \qquad \text{at } \xi = \xi_o = \frac{h_o}{h_m},$$

and
$$y = 0 \qquad \text{at } \xi = 1$$

yielding the equations

$$A_1 \sin \left(K \log_e \frac{h_o}{h_m}\right) + A_2 \cos \left(K \log_e \frac{h_o}{h_m}\right) = 0$$

and $\quad A_2 = 0$

Therefore, the stability conditions require

$$\sin \left(K \log_e \frac{h_o}{h_m}\right) = 0$$

from which the smallest non-trivial root is

$$K_1 = \frac{\pi}{\log_e h_o - \log_e h_m}$$

and the corresponding critical load is

$$P_{cr} = \mu \frac{\pi^2 E_t I_m}{L^2} \tag{3.22}$$

in which

$$\mu = \tfrac{1}{4} \left(1 - \frac{h_o}{h_m}\right)^2 \left[\frac{1}{\pi^2} + \frac{4}{(\log_e h_o - \log_e h_m)^2}\right] \tag{3.23}$$

The critical load is again analogous to that of a column with constant cross section having an equivalent moment of inertia

$$I = \mu I_m$$

3.3 Inelastic Buckling

The theory of elastic stability is based on the assumption that the stresses in the column would be below the elastic limit at the instant when equilibrium becomes unstable. In shorter columns the elastic limit is exceeded before the column becomes unstable. In such a condition, the equivalent modulus of elasticity becomes a function of the critical stress.

3.3a Double Modulus Theory

Considering a short column compressed by an axially applied load, P, so that $\sigma = \frac{P}{A}$ exceeds the proportional limit. Then let the load be further increased until the column reaches the condition of unstable equilibrium similar to that of elastic columns, and let it be deflected slightly. In every cross section there will be an axis, n-n, perpendicular to the plane of bending in which the cross-sectional stress developed prior to deflection remains unchanged. Bending will increase the compression stress on one side of the line n-n and decrease it on the other side. The rate of increase is proportional to $\frac{\partial\sigma}{\partial\varepsilon} = E_t$, and E_t is the tangent modulus of the stress-strain curve in Figure 3.5. Because the strain reversal relieves only the elastic portion of the strain, the reduction on the other side of n-n will be following the law of proportionality of stress and strain. The stress diagram on the convex side is bounded by the line, NA', (Figure 3.6) having a different slope from that of the line, NB'.

The equilibrium between internal stresses and external load requires

$$\int_0^{h_1} S_1 \, dA - \int_0^{h_2} S_2 \, dA = 0 \qquad (3.24)$$

and

$$\int_0^{h_1} S_1(z_1 + a) \, dA + \int_0^{h_2} S_2 \, (z_2 - a) \, dA = Py \quad , \qquad (3.25)$$

where: S_1 and S_2 denote the statical moments of the cross-sectional area to the left and right of the axis n-n, about this axis.

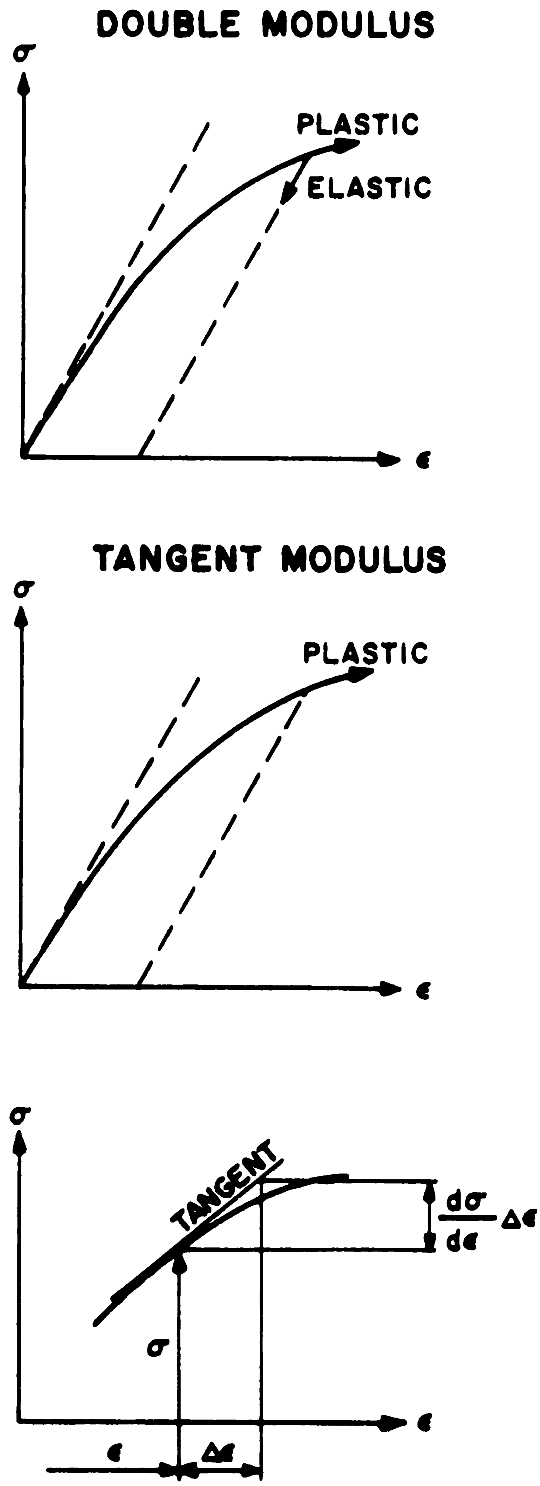

Figure 3.5--The double and tangent modulus theories of inelastic buckling.

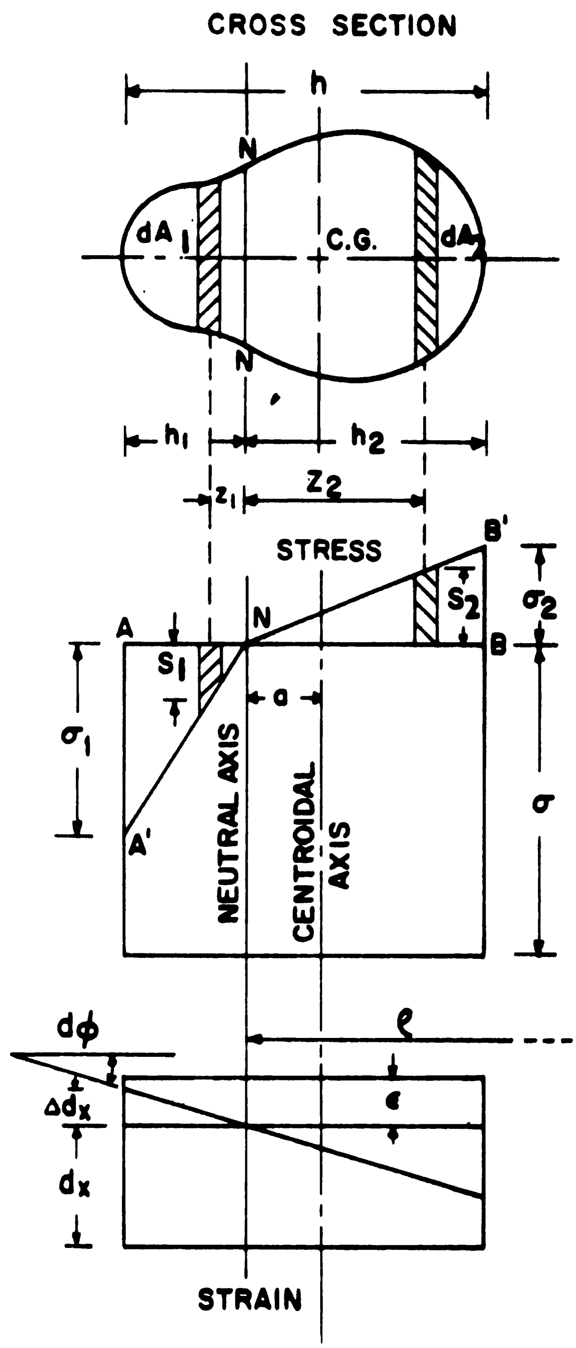

Figure 3.6--Stresses and strains in a section of an inelastic column subjected to axial loading.

a = the distance between the neutral and centroidal axis.

and y = the deflection, taken with respect to the centroidal axis of the column.

From Figure 3.6,

$$S_1 = \frac{\sigma_1}{h_1} z_1 \text{ and } S_2 = \frac{\sigma_2}{h_2} z_2$$

Also from the relative rotations of two cross sections in Figure 3.6:

$$\Delta\, dx = h_1\, d\phi$$

and since

$$\Delta\, dx = \frac{\sigma_1 dx}{E}$$

then

$$\frac{d\phi}{dx} = \frac{\sigma_1}{E_1 h_1} = \frac{\sigma_2}{E_2 h_2}$$

For small deformations $\frac{d\phi}{dx} = \frac{d^2y}{dx^2}$

therefore

$$\sigma_1 = E\, h_1 \frac{d^2y}{dx^2} \text{ and } \sigma_2 = E_t\, h_2 \frac{d^2y}{dx^2}$$

Therefore equation 3.24 becomes

$$E \frac{d^2y}{dx^2} \int_o^{h_1} z_1\, dA - E_t \frac{d^2y}{dx^2} \int_o^{h_2} z_2\, dA = 0$$

or

$$E\, S_1 - E_t\, S_2 = 0 \qquad (3.26)$$

This equation together with the relation, $h_1 + h_2 = h$, determines the position of neutral axis, n-n. The second equation, 3.25, yields

$$\frac{d^2y}{dx^2} \left(E \int_0^{h_1} z_1{}^2 \, dA + E_t \int_0^{h_2} z_2{}^2 \, dA\right)$$

$$+ a \frac{d^2y}{dx^2} \left(E \int_0^{h_1} z_1 \, dA - E_t \int_0^{h_2} z_2 \, dA\right) = Py$$

which results $\frac{d^2y}{dx^2} (E\, I_1 + E_t\, I_2) = P\, y$

where I_1 and I_2 represent the moments of inertia to the left and right of n-n respectively.

Introducing $\bar{E}\, I = E\, I_1 + E_t\, I_2$

results $$\bar{E} \frac{d^2y}{dx^2} + P_y = 0 \tag{3.27}$$

where: $$\bar{E} = E \frac{I_1}{I} + E_t \frac{I_2}{I}, \tag{3.28}$$

= the effective or double modulus

and I = the moment of inertia of the cross section about the axis through the center of gravity.

Once the stress-strain curve in compression is available, $\bar{E}$ can be determined by means of equations 3.26 and 3.28. In the inelastic range $\bar{E}$ is variable, while in the elastic range $\bar{E}$ becomes the same as E.

And as in section 3.2a, for straight column hinged from both ends, the critical load becomes

$$P_d = \frac{\pi^2 \bar{E} I}{L^2} \tag{3.29}$$

3.3b <u>Tangent Modulus Theory</u>

This theory was originated under the assumption that when the column buckles after being stressed beyond the elastic limit, no strain reversal takes place on the convex side of the bent column when it passes from the straight form to the adjacent deflected configuration.

Under this assumption the value of the tangent modulus, E_t, applies over the entire cross section. For axial loading, the differential equation of the deflected center line is

$$E_t I \frac{d^2y}{dx^2} + Py = 0, \tag{3.30}$$

and the critical load for the hinged ended column will be

$$P_t = \frac{\pi^2 E_t I}{L^2} \tag{3.31}$$

which is smaller than the value obtained from the double modulus theory. This value could be considered as a lower limit of the buckling load.

3.3c <u>Inelastic Buckling Model</u>

Crandall (1959) presented a simplified model that simulates the inelastic buckling conditions described in section 3.3a and 3.3b. The model, shown in Figure 3.7, consists of a rigid member supported by two strain hardened springs A and B. The force deformation relations for the springs has the same form as the stress-strain curve for the column material, Figure 3.7d.

Suppose that under the load, P, the system has reached the position where both springs have been compressed by δ_o, and the column remains straight, Figure 3.7a. Now suppose that only a small change is required to lead to the tipped position. There are two possible mechanisms by which this tipping can occur.

(i) <u>The double modulus mechanism</u>: where spring B is compressed a small additional amount while spring A decompresses (i.e., plastic loading and elastic unloading).

(ii) <u>The tangent modulus mechanism</u>: where both spring A and B suffer additional but unequal compression (i.e., further plastic loading).

<u>General Considerations</u>:

a. Considering the forces acting on the free body, Figure 3.7b, and assuming a small displacement, then

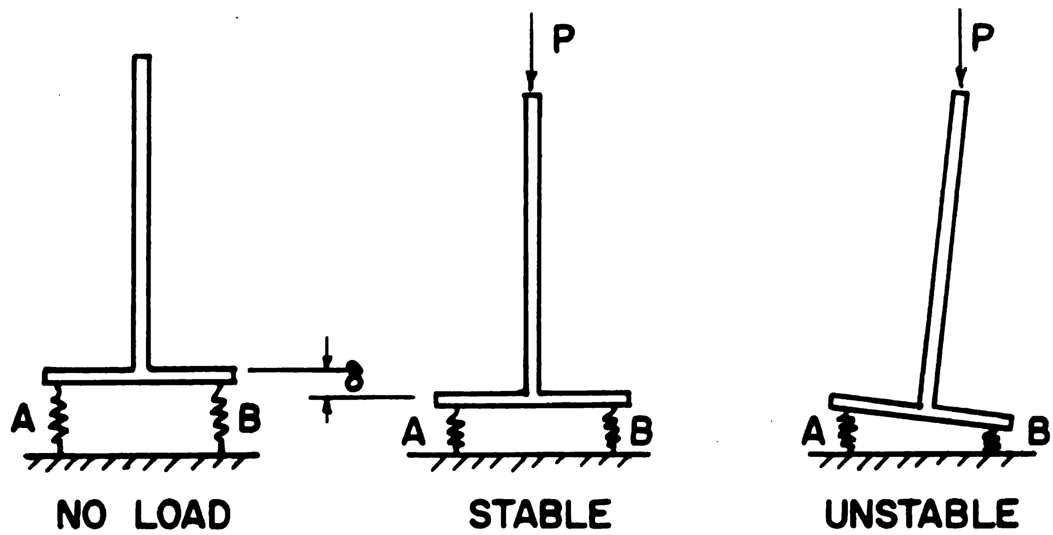

(a) Inelastic model with no load and under stable and unstable loading conditions.

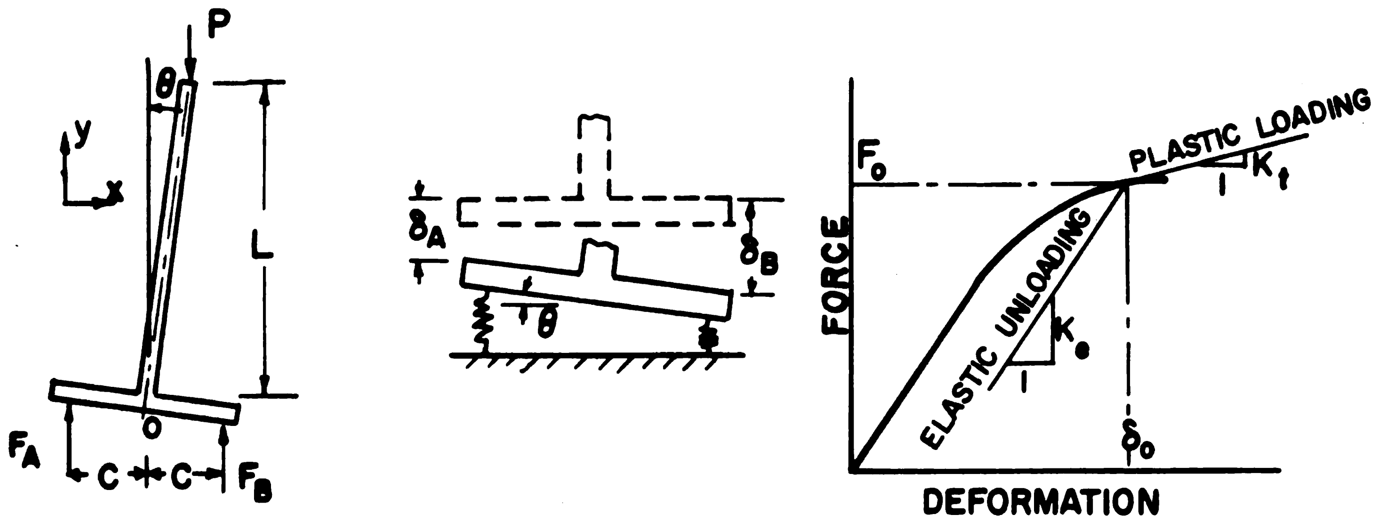

(b) Free body diagram

(c) Geometry of deformation

(d) Force-deformation curve of the column.

Figure 3.7--Inelastic buckling model.

$$\Sigma F_y = F_A + F_B - P = 0$$

and $$\Sigma M_o = - C F_A + C F_B - L \theta P = 0$$

or $$F_A = \frac{P}{2} (1 - \frac{L\theta}{C})$$

and $$F_B = \frac{P}{2} (1 + \frac{L\theta}{C})$$ } (3.32)

b. Considering the geometry of Figure 3.7c, the displacements of the two springs are related to the angle θ as follows

$$\delta_B - \delta_A = 2 C \theta \quad (3.33)$$

c. The plastic modulus, K_t, in a small neighborhood of δ_o, can be expressed approximately by the tangent of the curve at δ_o. Therefore

$F = F_o + K_t (\delta - \delta_o)$, represents the loading

and

$F = F_o - K_e (\delta - \delta_o)$, represents the unloading

where F_o = the force in each spring when the column is straight and the spring deflection is δ_o.

and

K_e = the slope of the elastic line of the force deformation curve.

With the above considerations in mind the loads at which the stability can exist are

$$P_d = \frac{2\ C^2}{L}\ \frac{2\ K_e\ K_t}{K_e + K_t}, \text{for the double modulus mechanism,} \quad (3.34)$$

and

$$P_t = \frac{2\ C^2}{L}\ K_t, \text{for the tangent modulus mechanisms.} \quad (3.35)$$

This model simulates the inelastic buckling once the force deformation behavior of the springs is similar to that of the original column material.

3.4 Inelastic Curved Hollow Tubular Column

Considering a given part of the straw as a hollow tubular column, it is possible to study the combined effect of initial curvature and inelastic behavior.

Assuming that the initial shape of the center line of the straw, Figure 3.8a, takes the shape:

$$y_1 = e \sin \frac{\pi x}{L} \quad (3.36)$$

And under the action of the compressive force, P, an additional deflection:

$$y_2 = \delta \sin \frac{\pi x}{L} \quad (3.37)$$

is produced. The change of the curvature at the middle of the straw is

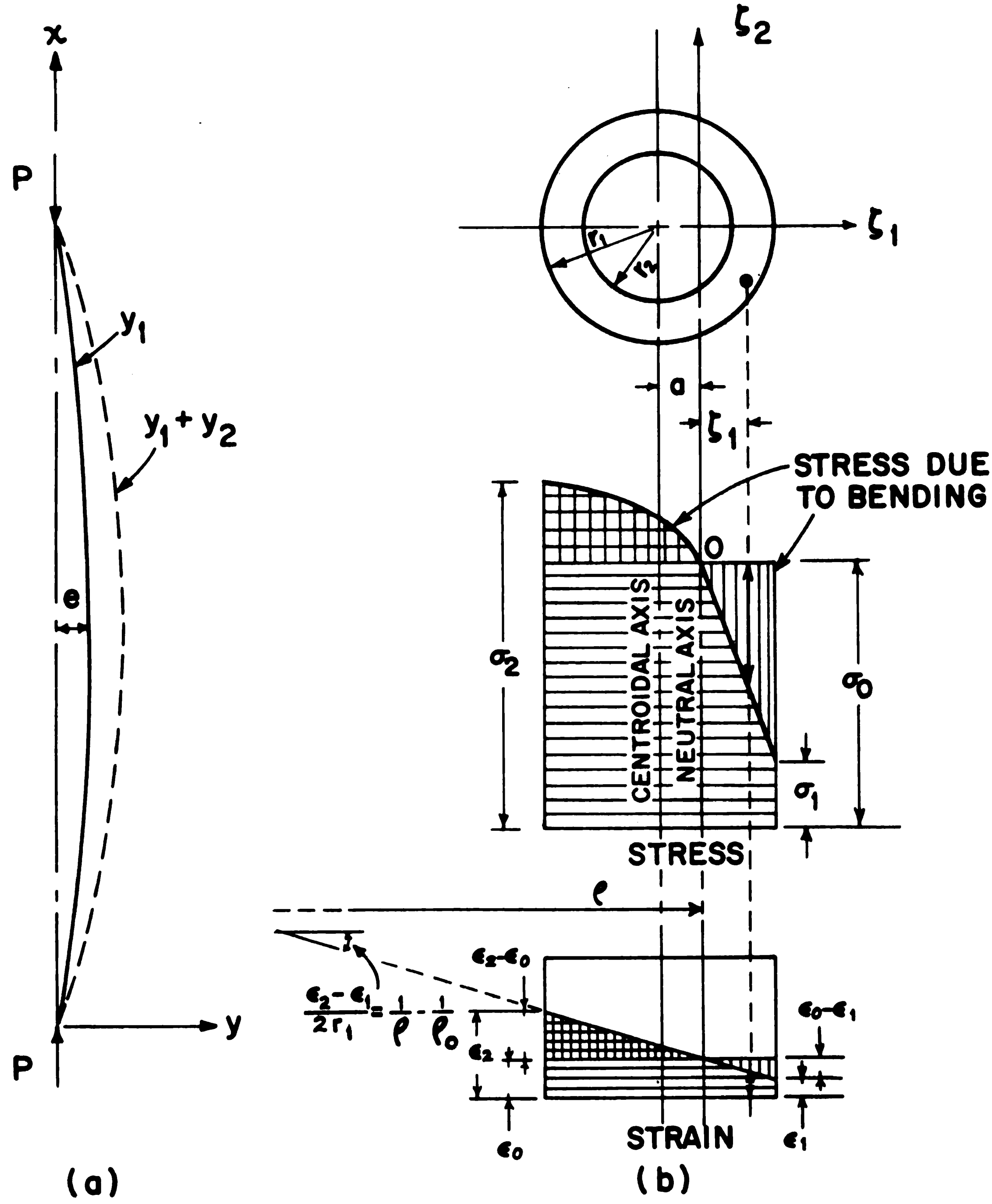

Figure 3.8--Inelastic curved hollow tubular column under axial loading.

$$\frac{1}{\rho} - \frac{1}{\rho_o} = -\left(\frac{d^2y_2}{dx^2}\right)_{x = L/2} = \frac{\delta\pi^2}{L^2} \qquad (3.38)$$

where $\frac{1}{\rho_o}$ = the initial curvature at $x = \frac{L}{2}$

Assuming that the strains in the outmost fibers at the middle of the straw are ε_1 and ε_2. The change of curvature, due to the deformation resulted from the longitudinal force, P, can also be written as

$$\frac{1}{\rho} - \frac{1}{\rho_o} = \frac{\varepsilon_2 - \varepsilon_1}{2r_1} \qquad (3.39)$$

where ρ_o = the initial radius of curvature

and ρ = the radius of curvature of the section under consideration.

From the last two equations the additional deformation, δ, can be obtained for any assumed values of ε_1 and ε_2,

$$\delta = \frac{L^2}{\pi^2}\,\frac{\varepsilon_2 - \varepsilon_1}{2r_1} \qquad (3.40)$$

Also the compressive force, P, from the equation

$$\sigma_c = \frac{P}{Area} = \frac{1}{\varepsilon_2 - \varepsilon_1}\int_{\varepsilon_1}^{\varepsilon_2} \sigma d\varepsilon \qquad (3.41)$$

and the bending moment is related to the total deflection as follows

$$P\,(e + \delta) = M \qquad (3.42)$$

Since bending and direct stress occur simultaneously from the beginning and grow together with increasing load P, no strain reversal is presumed to occur on the convex side of the deflected straw at the instant at which the critical load is reached. When P increases until the proportional limit is exceeded in the entire cross section, or at least in the highest stressed portion of the section, the stress distribution will follow the stress-strain diagram for the straw. As shown in Figure 3.8b, every section will have a σ_o axis along which the stress equals the average stress $\frac{P}{A}$, i.e.,

$$\sigma = \sigma_o = \frac{P}{A} .$$

Considering the total stress, σ, consisting of two parts σ_o, and the stress due to bending denoted by σ_b, then

$$\sigma = \sigma_o + \sigma_b . \tag{3.43}$$

In Figure 3.8b, the condition of equilibrium requires

$$\int_{-r_1-a}^{r_1-a} \int_{o}^{\sqrt{r_1^2 - (\zeta_1 + a)^2}} \sigma_b \, d\zeta_2 d\zeta_1 - \int_{-r_2-a}^{r_2-a} \int_{o}^{\sqrt{r_2^2 - (\zeta_1 + a)^2}} \sigma_b \, d\zeta_2 d\zeta_1 = 0 \tag{3.44}$$

and

$$\int_{-r_1-a}^{r_1-a} \int_{0}^{\sqrt{r_1^2 - (\zeta_1 + a)^2}} \sigma_b \quad \zeta_1 d\zeta_2 d\zeta_1 \quad - \int_{-r_2-a}^{r_2-a} \int_{0}^{\sqrt{r_2^2 - (\zeta_1 + a)^2}} \sigma_b \, \zeta_1 d\zeta_2 d\zeta_1 = \tfrac{1}{2}P(y_1 + y_2)$$

(3.45)

where, as shown in Figure 3.8b

ζ_1 = the distance of a fiber from the σ_o-axis of the cross section.

a = the distance between the centroidal axis and the σ_o axis.

Also in Figure 3.8b, the stresses and corresponding strains are: ε_o = the compressive strain corresponding to the average stress σ_o.

$\varepsilon_1, \varepsilon_2$ = the minimum and maximum compressive strains, respectively, corresponding to the compressive stresses σ_1 and σ_2 at the external fibers.

Let us consider the relative rotation of two cross sections a distance unity apart, and in reference to Figure 3.8b,

$$\varepsilon - \varepsilon_o = \frac{\zeta_1}{\rho} \qquad (3.46)$$

and

$$\frac{\varepsilon_2 - \varepsilon_1}{2r_1} = \frac{1}{\rho} - \frac{1}{\rho_o} \qquad (3.47)$$

From equations 3.46 and 3.47 we can write

$$\zeta_1 = \frac{2\ r_1\ \rho_o\ (\varepsilon - \varepsilon_o)}{2\ r_1 + \rho_o\ (\varepsilon_2 - \varepsilon_1)} \tag{3.48}$$

Differentiation with respect to ζ_1 yields

$$d\varepsilon = \left(\frac{\varepsilon_2 - \varepsilon_1}{2\ r_1} + \frac{1}{\rho_o}\right) d\zeta_1 \tag{3.49}$$

Using equations 3.48 and 3.49 together with equations 3.44 and 3.45, we can write

$$\int_{\varepsilon_1}^{\varepsilon_2} \int_0^{\sqrt{r_1^2 - \{\frac{2r_1\rho_o(\varepsilon-\varepsilon_o)}{2r_1 + \rho_o(\varepsilon_2-\varepsilon_1)} + a\}^2}} \sigma_b \quad d\zeta_2 d\varepsilon - \int_{\varepsilon_1}^{\varepsilon_2} \int_0^{\sqrt{r_2^2 - \{\frac{2r_1\rho_o(\varepsilon-\varepsilon_o)}{2r_1 + \rho_o(\varepsilon_2-\varepsilon_1)} + a\}^2}} \sigma_b \quad d\zeta_2 d\varepsilon = 0$$

$$(3.50)$$

and

$$\int_{\varepsilon_1}^{\varepsilon_2} \int_0^{\sqrt{r_1^2 - \{\frac{2r_1\rho_o(\varepsilon-\varepsilon_o)}{2r_1 + \rho_o(\varepsilon_2-\varepsilon_1)} + a\}^2}} \sigma_b(\varepsilon-\varepsilon_o)\ d\zeta_2 d\varepsilon - \int_{\varepsilon_1}^{\varepsilon_2} \int_0^{\sqrt{r_2^2 - \{\frac{2r_1\rho_o(\varepsilon-\varepsilon_o)}{2r_1 + \rho_o(\varepsilon_2-\varepsilon_1)} + a\}^2}} \sigma_b(\varepsilon-\varepsilon_o)\ d\zeta_2 d\varepsilon$$

$$= \frac{\{2r_1 + \rho_o(\varepsilon_2-\varepsilon_1)\}^2}{8r_1^2\ \rho_o}\ P(y_1 + y_2)$$

$$(3.51)$$

In these equations σ_b should be considered a function of ε represented by the portion of the stress-strain curve which lies between ε_1 and ε_2 (Figure 3.8b).

For a given average stress, $\sigma_o = \frac{P}{A}$, and a given maximum compressive strain, ε_2, on the concave side of the column, equation 3.50 yields the minimum compressive strain ε_1. Similarly a set of various distributions of stress pertaining to the same axial load, P, can be determined, representing possible distributions of stress which may exist at the various cross sections of the bent column. For each of these stress areas a value of radius of curvature can be determined through equation 3.47. In this manner a set of correlated values, ρ and y , can be obtained defining a function $\rho = f(y_1, y_2)$. And since for small a deflection, $\frac{1}{\rho} = \frac{d^2y}{dx^2}$, the following relationship can be established:

$$\frac{d^2y}{dx^2} = f(y_1, y_2) \; . \qquad (3.52)$$

Such a differential equation defines y, the shape of the centerline, for any value of $\sigma_o = \frac{P}{A}$, initial shape y_1, and length of the straw.

Bleich (1951) reported a typical relationship between the average stress, σ_o, and the deformation, y_m, at the midheight of a straight column with a rectangular solid cross section, made of elastic plastic material now, eccentrically loaded. In such a situation of a eccentrically loaded elastic-plastic column, the relation between σ_o and y_m will be similar to that of Figure 3.9. From this relation, some observations can be made. At the stress σ_o, two configurations of equilibrium are possible, both pertaining to the same load $P = A\sigma_o$. One configuration corresponds to a stable deflection, where an increase in σ results in an increase in the deflection. This configuration exists after the load, P, is removed and the column returns toward its original shape. However, it retains a slightly bent shape due to the residual plastic strain in those fibers where the proportional limit was exceeded. The second configuration is unstable; since a further increase in y_m involves reduction of σ_o.

The maximum value of stress, σ_c, indicates, therefore, the transition from stable to unstable equilibrium. Accordingly, $P_{cr} = A\sigma_c$ defines the failure load of the eccentrically loaded column. It should be clear, from this reasoning, that the failure is not due to reaching a certain critical fiber stress, but because the stable equilibrium is no longer possible between the internal and external bending moment.

In the limiting case of straight column, i.e., no initial curvature, the σ_o - y_m curve assumes the shape indicated by the dashed curve of Figure 3.9. The critical load is then the load obtained from the tangent modulus theory.

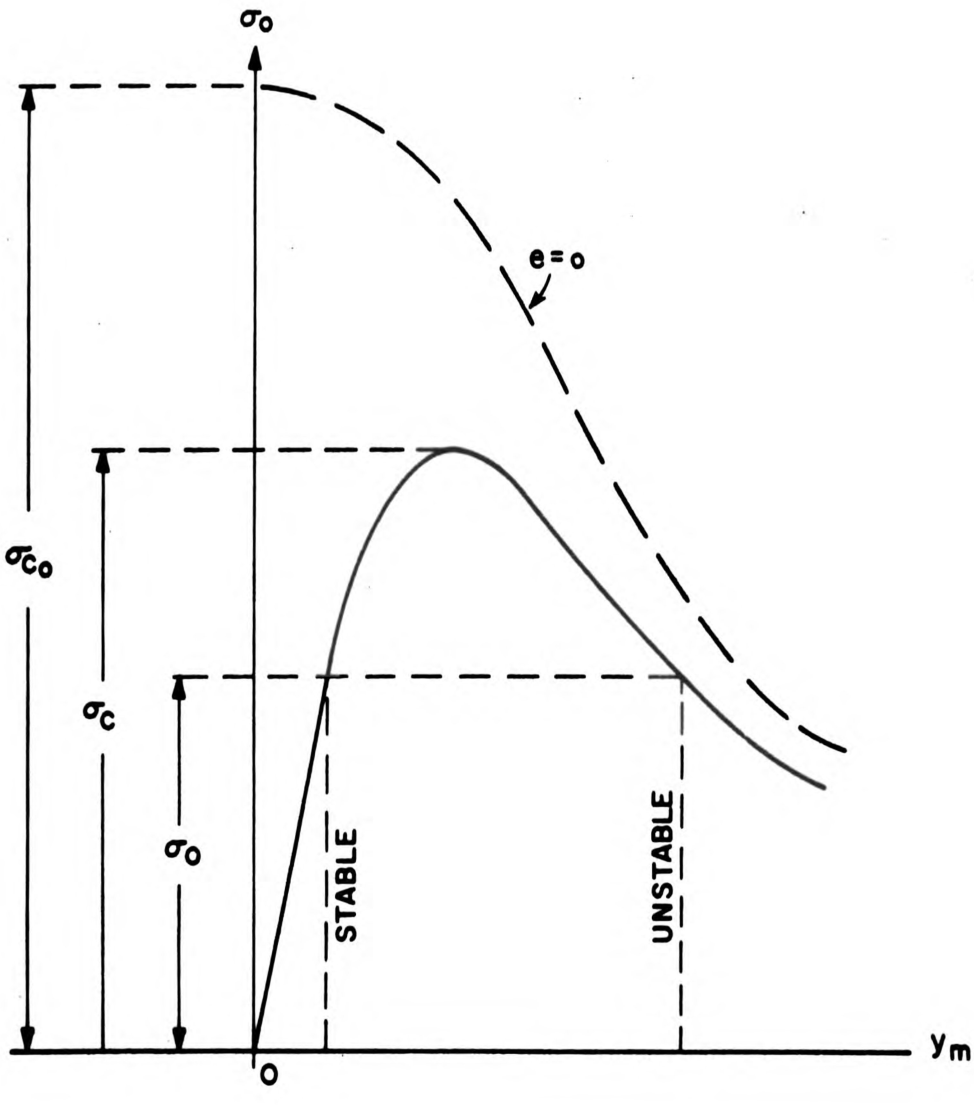

Figure 3.9--The relation between the axial stress and the deformation of the centriodal axis at the middle of the column.

4. EXPERIMENTAL PROCEDURE AND EQUIPMENT

In agricultural engineering research, two approaches are commonly used: (a) the factorial analysis, i.e., isolating the different factors affecting certain phenomena and checking each one of them separately, and (b) the utilization of information or techniques available from other engineering areas. The second approach is being used in this study.

To determine experimentally the mechanical and rheological properties of an agricultural material, it is necessary to have some means of measuring applied stresses and the amount of strain as a function of time. It is also highly desirable to have a recording unit to provide a continuous and permanent record to the existing relationships. It was recognized from preliminary tests that the cereal grain plant has viscoelastic behavior, and as such its behavior would be considerably influenced by temperature and humidity conditions. Therefore, a temperature and humidity controlled testing chamber was utilized.

4.1 Equipment

4.1a Testing Chamber

The testing chamber was six feet wide, eight feet long, and seven feet high. It was previously constructed of two layers of plywood between which fiberglass insulation was fitted. The temperature was controlled by means of a thermostat operated air conditioner located in the lower front corner of the chamber. With an air duct fitted to it, it directed the air toward the top of the chamber to minimize temperature gradient and to reduce air movement in the area where the samples were tested.

The humidity was controlled by means of a humidistat operated solenoid in a low pressure steam line entering the chamber through a horizontal 20-inch long half-inch pipe. The pipe had small holes drilled at one-inch spacing along the top.

Throughout the tests the temperature was maintained at 72 ($\pm$ 3) degrees F., and the humidity was held at 65 ($\pm$ 4) percent.

4.1b The Testing Machine and Recording Unit

The overall view of the testing machine and recording unit is shown in Figure 4.1. The basic unit of this machine, which was assembled previously by Finney, was a 4-inch stroke, double acting, pneumatically driven air motor with positive, hydraulically controlled piston speed in both directions. The machine was capable of producing forces in

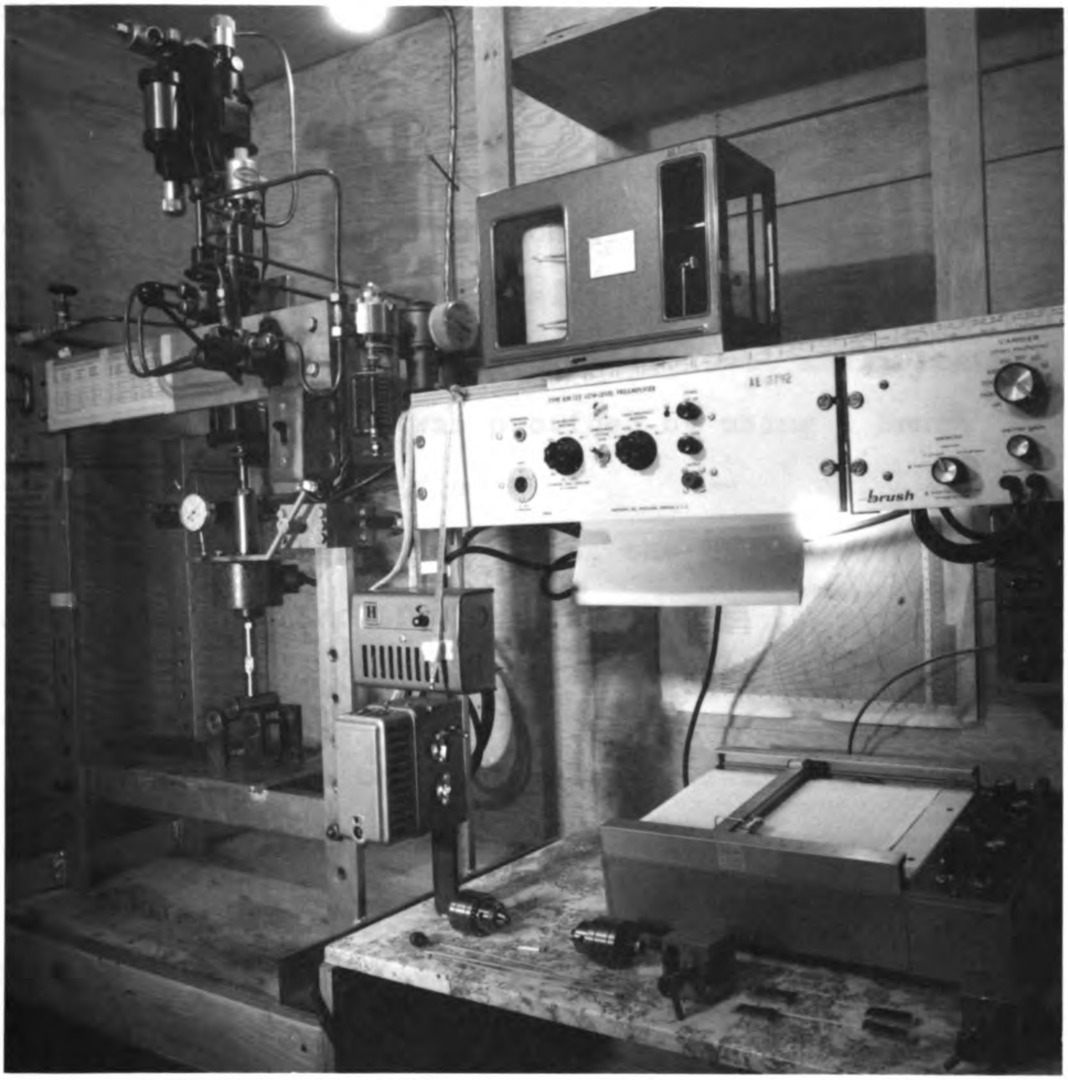

Figure 4.1--Overall view of the testing machine and recording unit.

tension and compression of about 300 pounds at constant strain rates which may be varied from zero to about 50 inches per minute.

4.1c Stress Measurement

During the tests, the encountered forces were measured by a Baldwin-Lima-Hamilton U-1B 50-pound capacity load cell and recorded by a Mosley 135 X-Y recorder. Due to the low range of forces used, additional amplification of the load cell output was provided by using a Brush strain gage bridge amplifier.

Before each series of tests, the calibration of the load cell and the amplifier was checked.

4.1d Strain Measurements

In most of the tests, it was necessary to check the relaxation characteristics of the tested specimen. For this reason these tests were conducted in two parts: (1) a constant strain rate loading followed by, (2) stress relaxation test while the specimen was held at constant deformation. During the loading phase displacements were measured using a dial gage at the load cell. The observed displacements were recorded using an event marker on the X-Y recorder.

This method of strain measurement gave the relative displacement between the load cell and the base of the testing machine. This means that the strains within the mountings were also included. As indicated later, it became necessary for some of the tests, especially the compression tests, to search for another method of measuring the strains within the specimen itself.

Because of the difficulty of mounting any strain measuring devices on the wheat plant specimen itself and the small forces used in most of the tests, it became necessary to utilize a method that does not include touching the tested specimen.

An optical strain measurement method was developed. This method proved useful for strain measurement in the compression test. In this optical method two marks, one-half of an inch apart, were made on the straw specimen, and while the load was applied successive photographs were taken at defined intervals. A mark, corresponding to each picture, was recorded on the loading curve using the event marker on the X-Y recorder. The photos were taken with a 35-millimeter camera at a fixed distance of about 4.5-inches from the tested specimen. The change in the distance between the two marks on the straw was measured by projecting the negative and producing sufficient enlargement to give reasonably accurate measurements.

4.2 Laboratory Tests

In order to determine the mechanical and rheological behavior of wheat plants under different loading conditions, it was necessary to conduct a series of strength tests. Compression, tension, and bending tests were made. For the purpose of studying the stability of the plant, buckling tests were also carried out. In each of these tests two parts of the plant were tested. The first part was that immediately below the head, and the other was the lower portion of the plant just above the ground.

Three varieties of the wheat plant (Triticum Vulgarus) were tested over a four-week period starting one week before the early harvesting season of 1965. The varieties tested were Comanche, Redcoat, and Genesee. Six samples, from three plants, were tested in each experiment.

The samples were obtained from the field in the morning and stored in the temperature and humidity controlled testing chamber. The samples then were prepared and tested in the same day. With each test, a moisture content and linear density test were made. Also, the cross-sectional dimensions, the outer diameter and thickness of the sample was measured (Figure 4.3). Figure 4.2 shows the samples prepared for testing.

4.2a Tension and Compression Tests

In order to determine behavior of the wheat stem in tension, three-inch samples were tested from the top and lower portion of the plant stem. Each sample was clamped from both sides by two 1/4 of an inch plywood blocks covered with sand paper to prevent the sample from slipping. The distance between the two clamps was about one-inch. The recording procedure was such that the recording pin moves

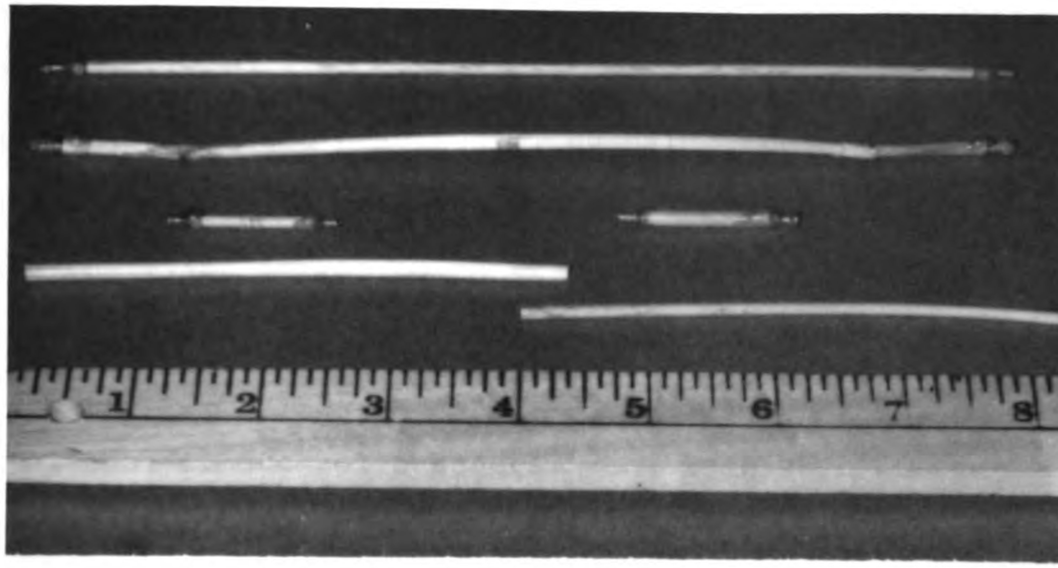

Figure 4.2--Samples prepared for testing.

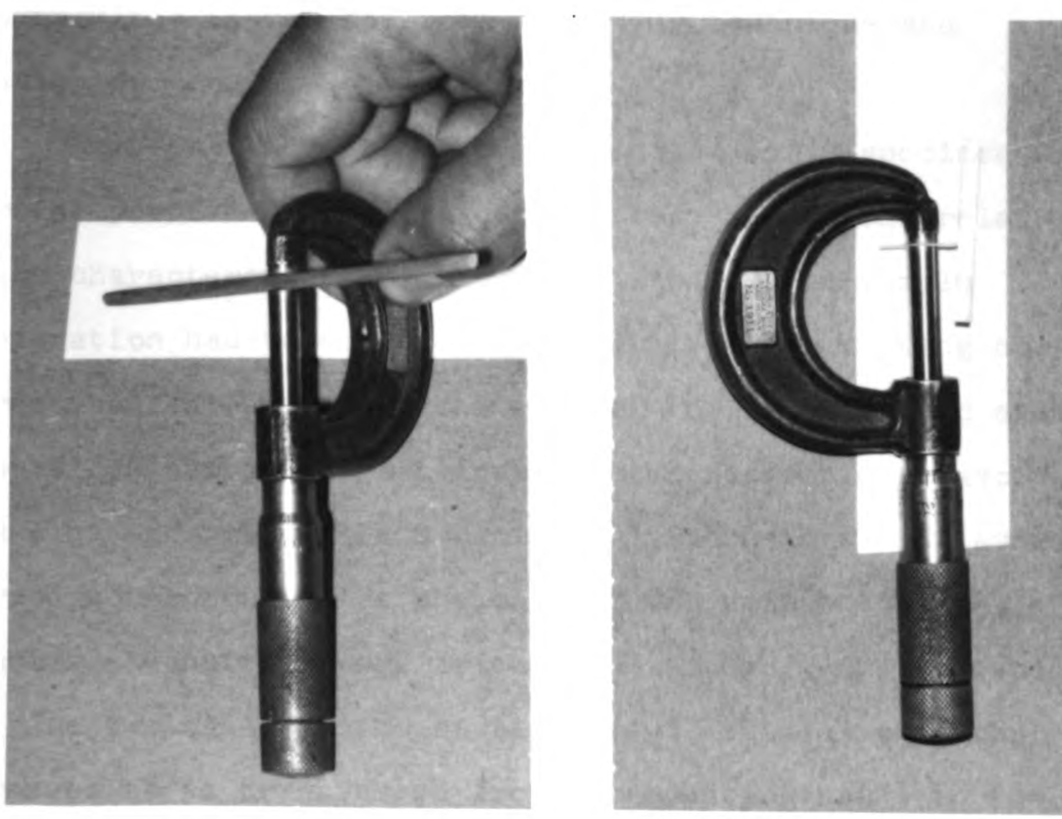

Figure 4.3--Measurements of the cross section of the test specimen.

in the x-direction at a constant rate while the resulting force was recorded on the y-axis. The deformation was measured, as stated previously, by using the dial gage at the load cell. The observed displacement was recorded using the event marker on the X-Y recorder. In fact, this displacement was that of the piston rod. This includes any relative movement between the specimen and the supporting clamps, if such slip occurs. The length of tested specimen, i.e., the distance between the two supports, and the cross-sectional dimensions, the outer diameter and wall thickness, were recorded for each sample. Figures 4.4 and 4.5 show the tested specimen, mounting technique and testing procedure.

Compression tests were made on the straw specimen for the purpose of obtaining the stress-strain and relaxation characteristics of the wheat straw. The sample preparation had to be made such that neither buckling nor stress concentrations at the ends of the sample would exist. A one-inch sample was considered to be desirable to avoid buckling and yet not be too difficult to handle. To avoid stress concentration at the ends of the sample, several mounting techniques were tried. The chosen technique was to glue two nails inside of the straw. This allowed the stresses to be transferred from the mounting nails to the straw through the bond. Figures 4.6 and 4.7 show the compression test samples before and after preparation for testing. The test was conducted in two parts: (1) a

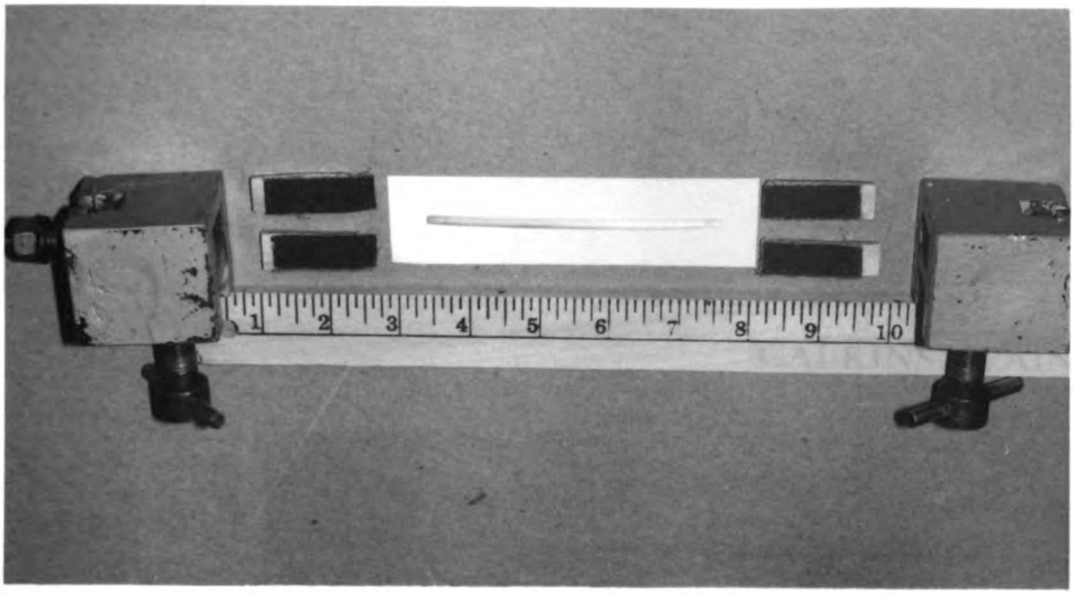

Figure 4.4--Method of mounting samples for tension test.

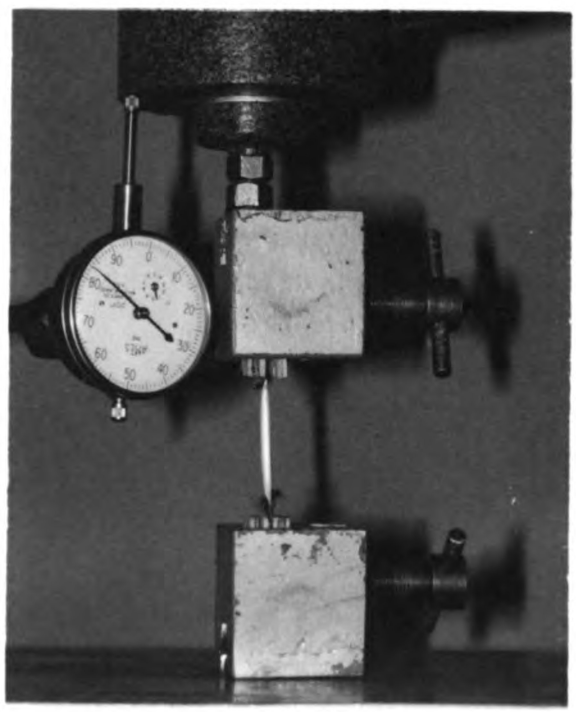

Figure 4.5--The tension test.

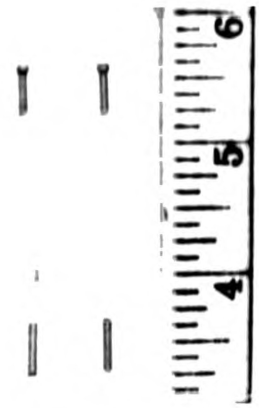

Figure 4.6--Straw specimen for compression test.

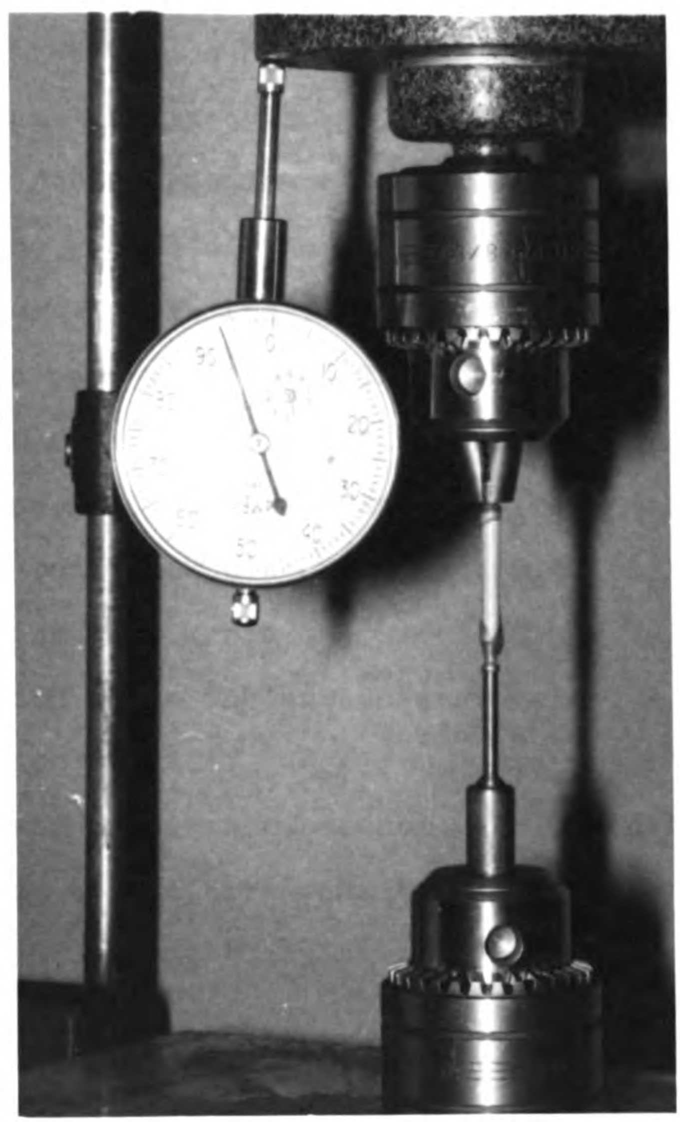

Figure 4.7--Uniaxial compression test.

constant strain rate loading followed by, (2) stress relaxation test while the specimen was held at constant deformation. And, as in the tension test, during the loading phase displacements were measured, using the dial gage at the load cell, and recorded on the chart using the event marker on the X-Y recorder. This measured displacement should include all the strain in the mounting nails, and supporting bond. And as will be mentioned in the next chapter, this was the reason behind the lower values of moduli of elasticity obtained from compression tests.

During the loading portion of the test the force was recorded on the y-axis of the X-Y recorder while the recording pin was moving in the x-direction at a constant rate of 20 seconds per each inch. The force was applied at a constant rate of about 0.01 $\pm$ 0.005 inches per minute.

The second part of the test was the stress relaxation test. This test took place at the end of each constant strain loading test where the specimen was held at constant deformation while the encountered force was recorded as a function of time.

Another strain measurement method, the photostrain technique, was used to avoid the additional strains from the mounting areas (Section 4.1d).

4.2b Bending Test

Because of problems encountered in mounting and strain measurements together with the time required for sample preparations, during which some changes in moisture content of the sample is expected to take place, the bending test was proved to be much more convenient and reliable. The test was conducted by loading the specimen as simply supported beam as shown in Figure 4.8. The force was applied at a constant strain rate. Throughout the tests the loading rate was in the range of 0.009 and 0.027 inches per minute. The sample supporting frame, as shown in Figure 4.8, consisted of two fixed and one moveable support in the middle. The encountered force and displacement at the middle of the tested specimen was measured by means of the load cell and dial gage.

As in the compression test, the bending test consisted of two parts: (1) constant strain rate loading, and (2) stress relaxation test during which the specimen was held at constant deformation. Also, the time base of the recorder was used for both deformation and relaxation measurements.

4.2c The Buckling Test

The stability of the wheat plant under axial load was also studied. An 8-inch specimen was selected because of the limits of the testing machine. Loads were applied at a constant rate of strain until the critical buckling load was reached. Two mounting techniques were employed in the stability tests. The first, as shown in Figure 4.9, was similar to that used in the compression

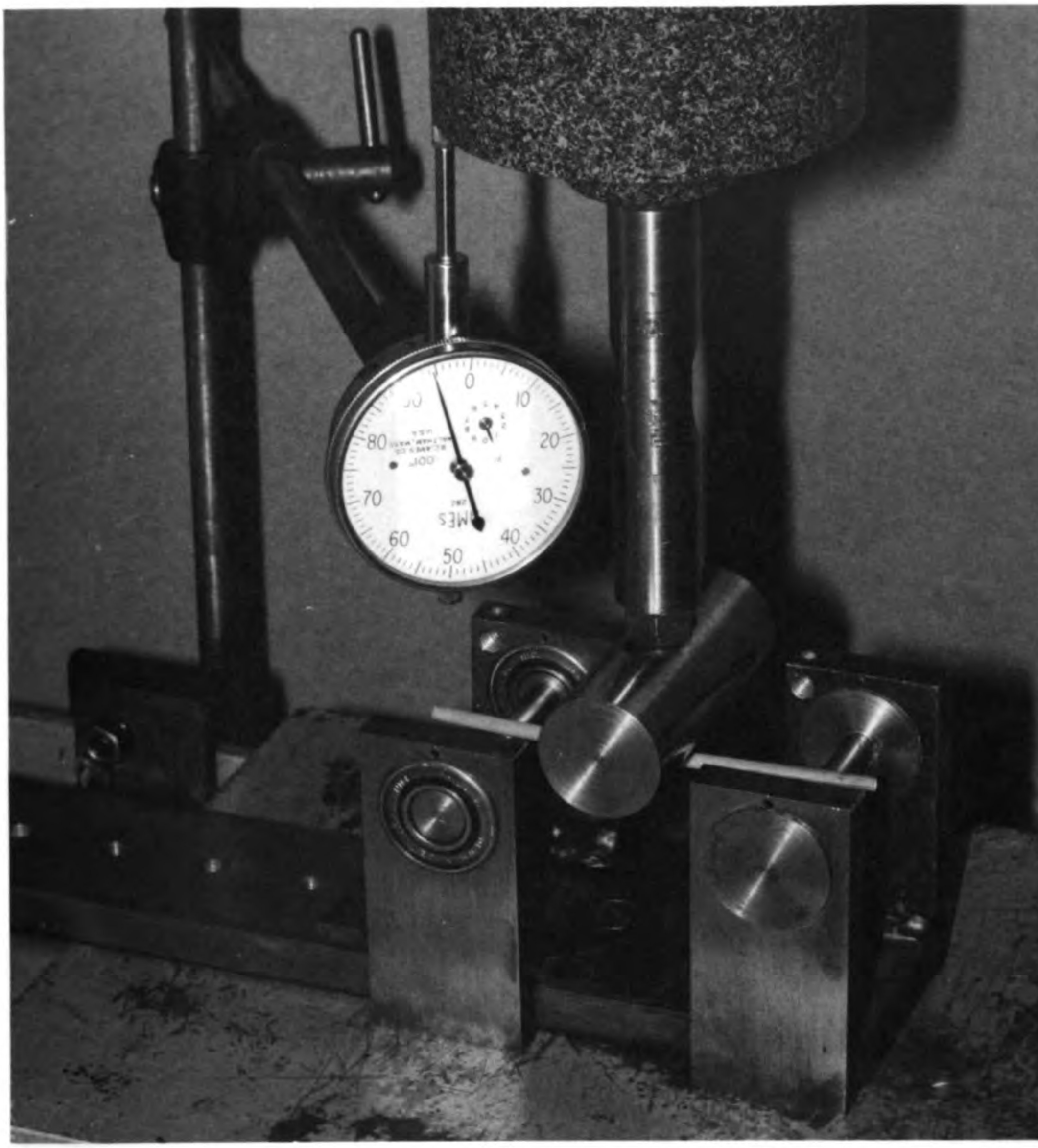

Figure 4.8--The Bending Test.

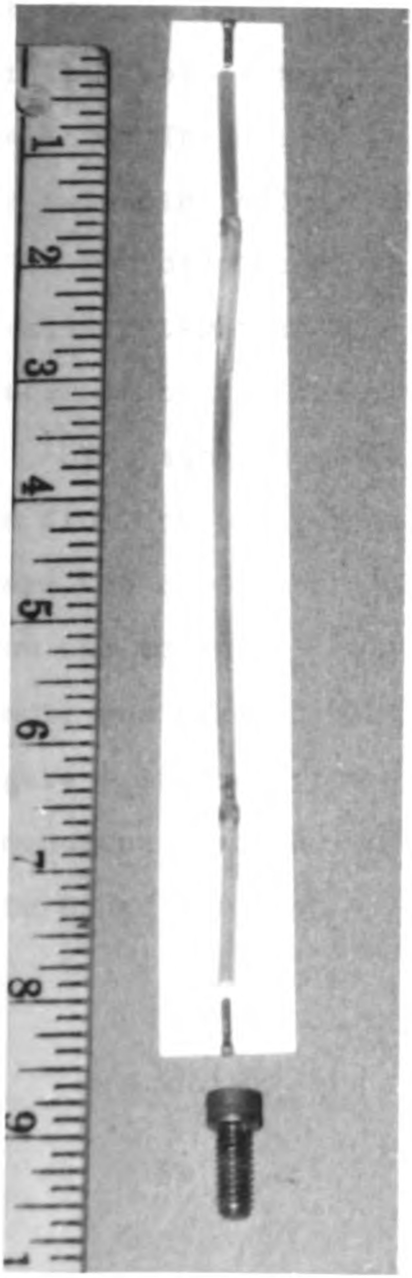

Figure 4.9--Method of mounting samples for buckling test.

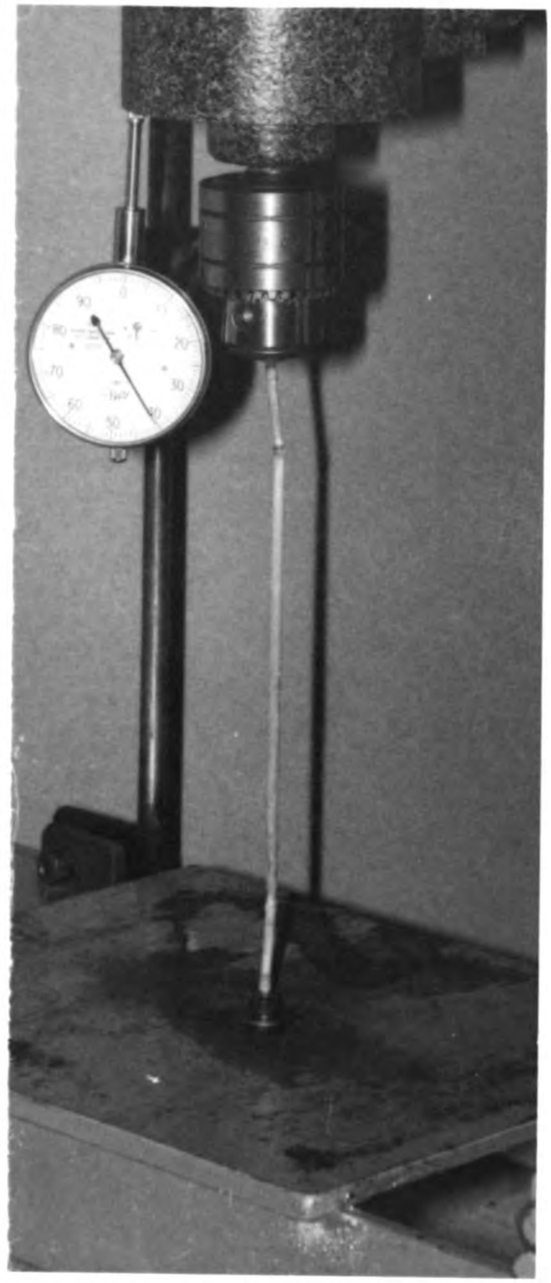

Figure 4.10--The buckling test.

test, where nails were fitted and bounded to the ends of the specimen for the purpose of preventing a failure at the ends of the specimen. This technique was desirable for the tests where the samples did not have a node at the end. The second technique, without fitted nails, was suitable for the samples which had nodes at the end.

The displacements of the ends were recorded, and a 16-millimeter film was taken for the purpose of checking the shape of the deformation.

Two samples were tested from each plant; the first was from the portion immediately under the plant head where the cross-sectional dimensions decrease gradually from the top node toward the plant head. The second sample was taken from the lower portion of the plant. Figure 4.10 shows the buckling test. The cross-sectional dimensions, length, and initial shape of each sample were determined for each test.

5. RESULTS AND DISCUSSION

5.1 General Characteristics of the Plant Behavior Under Applied Loads

It was clear from the force-deformation curves that the wheat straw does not react to applied stresses in a purely elastic manner. It was also observed that the loading curves of most of the tests had a plastic-like behavior. The shape of the stress relaxation curves confirmed the assumption that the wheat plant has some viscous properties. The moisture content and linear density of the tested plant were evaluated over the testing period, (Figure 5.1).

5.1a Tension and Compression Tests

Tension curves showed an approximately linear stress-deformation relationship. Compression curves, Figure 5.2a, however, showed a significant plastic-like behavior in the loading curves. The stress relaxation test showed the existance of significant damping effect. And as will be shown in section 5.2, it is possible from the loading and relaxation curves to obtain the necessary information about the elastic and viscous moduli of the tested specimens. After checking the damping characteristics of the wheat straw, as will be explained in section 5.2, the slope of

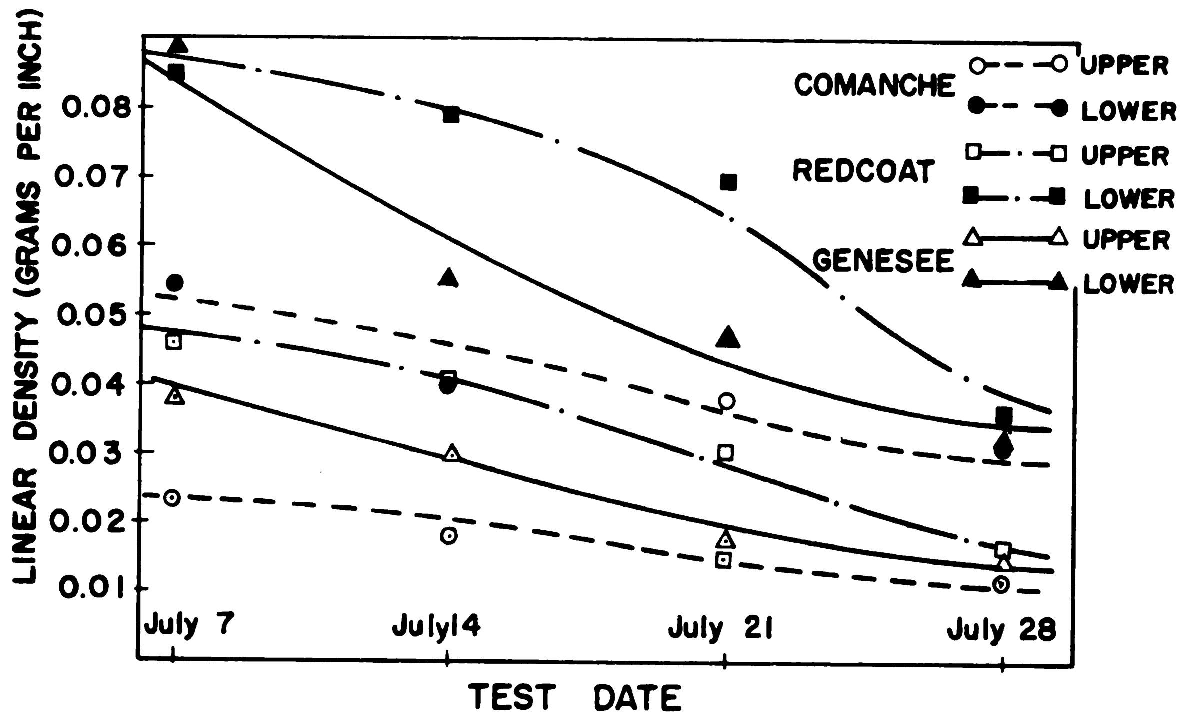

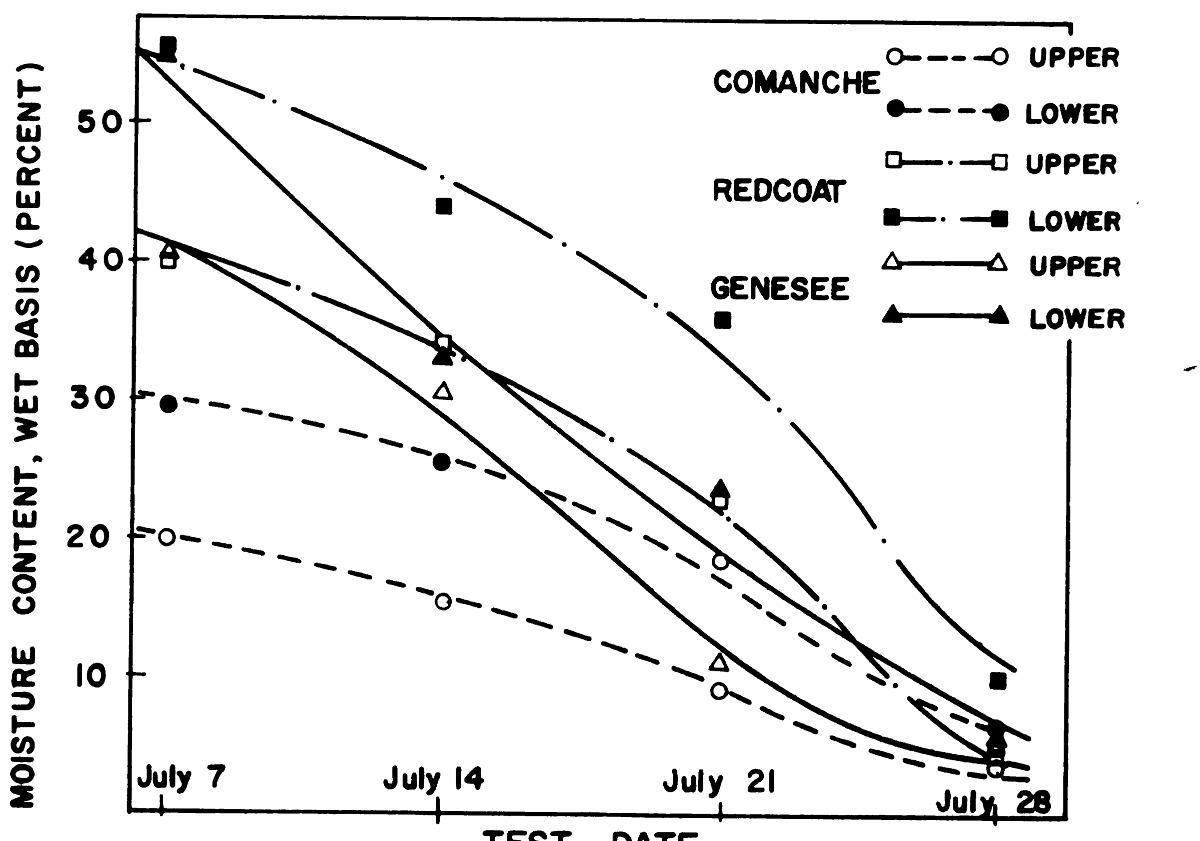

Figure 5.1--Moisture content and linear density of the samples over the testing period.

(a) Compression test

(b) Bending test

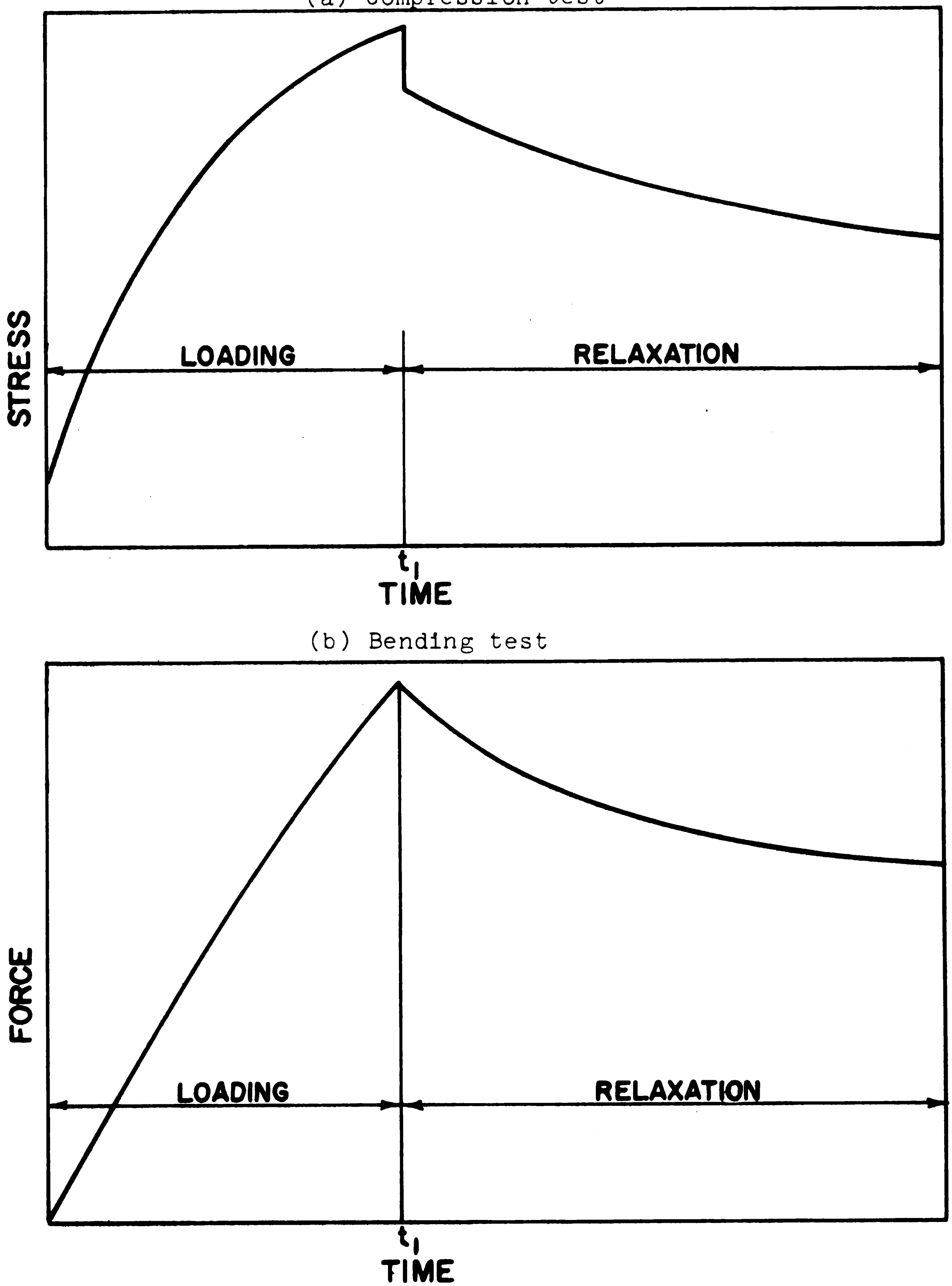

Figure 5.2--Typical behavior of loading and relaxation curves obtained from the compression and bending tests.

the first part of the loading curve was used to obtain the modulus of elasticity of the test specimen. Appendix Tables A-1 and A-2 show the obtained values of the modulus of elasticity from the tension and compression tests respectively.

From the first test, in comparing the obtained values for the modulus of elasticity from tension and compression to that obtained from the bending test, it was clear that the modulus of elasticity was much lower than expected from the results of the bending tests. The main reason for that was the larger values of measured strains than that within the specimen itself. This was mainly due to slip in the tension test, and strains within the mounting area in the compression test.

In order to reduce the error in strain measurement, the photo-strain measurement technique was developed. Three different samples were tested, and their stress-strain curves are shown in Figure 5.3. Appendix Table A-3 gives the data obtained from this technique. The values of the modulus of elasticity obtained from this technique were considerably higher than those obtained from the mechanical strain measurement and seems to be a practical method for such delicate materials as the wheat straw. It also lacked some sensitivity for short periods. Even after expanding the recorded view about 70 times larger than actual length, the change in length was small and quite difficult to make a precise measurement of the

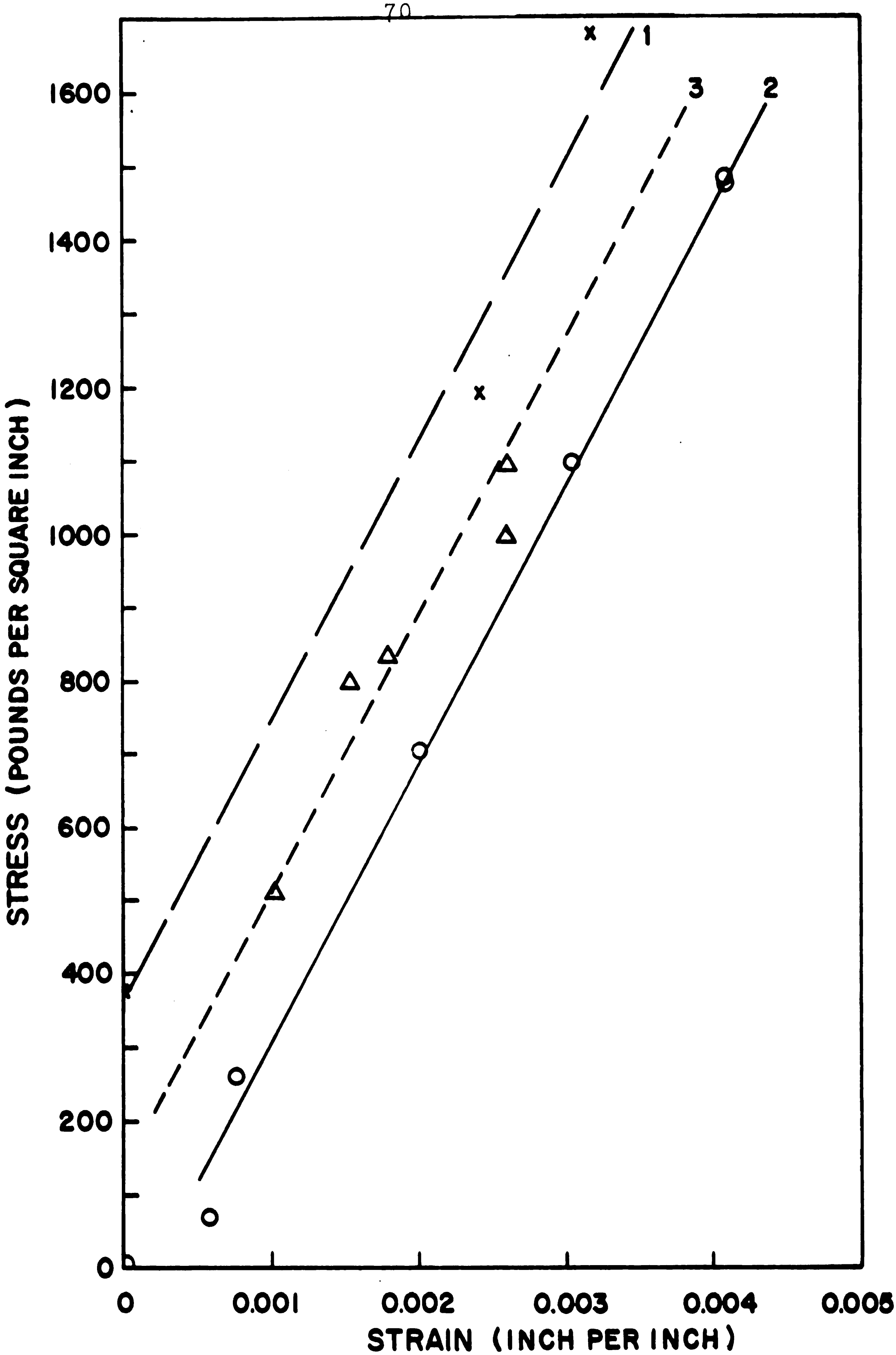

Figure 5.3--Stress-strain curves obtained from three samples by using optical strain measurement technique.

expanded photo. The accuracy could be improved if very sharp and dark marks are made, together with using a high sensitivity and better quality film.

5.1b Bending Test

In this test, all specimens were supported as simple beams and center loaded at constant rate of deformation. The encountered force and displacements of the middle point were recorded. The force-displacement relation was visibly non-linear. The amount of non-linearity of the relation depended on the amount of damping in the straw. At the end of the loading operation the material was allowed to relax while the deformation was held constant. A typical loading and relaxation curve for the wheat straw in bending is shown in Figure 5.2b. As will be shown in section 5.2, the slope of the first portion of the loading curve of a viscoelastic material can be used to obtain the elastic modulus of a tested specimen. For a simply supported beam with a force acting in the middle, the displacement, y, in the direction of the force is expressed as

$$y = \frac{F\,L^3}{48\,E\,I},$$

where: F = the applied force

L = the length of the specimen (distance between fixed supports)

I = the moment of inertia of the sample cross section

E = the modulus of elasticity

or
$$E = \frac{F\ L^3}{48\ I\ y}\ .$$

This relation was used to calculate the modulus of elasticity of the specimen. Appendix Table A-4 shows the calculated value of E from the bending tests over the four week period of tests. As shown in the table, the data obtained from a given test in the same period of time and for the same variety, give different values of E. The variation from one plant to another is a typical problem encountered in research on biological materials. If the aim of a given research is to obtain statistical data regarding a given characteristic, a large number of samples should be tested depending on the amount of variation that exists. In this study the main objective, however, was to explore the behavior of the plant and to express its behavior in terms of the engineering language. For this reason, only three samples were tested in each experiment.

It was also observed that after exceeding a certain amount of deformation, the cross section immediately under the applied force started to change from a circular to a rather elliptical shape. This flattening resulted in a reduction in the moment of inertia of the cross section and therefore less resistance to deformation.

The values of modulus of elasticity obtained from the bending test was used to check the assumed buckling model. Because of the variation from one plant to another, the value of E obtained from averaging three tests was not expected to be necessarily the exact value of the modulus of elasticity of the sample being tested for stability. It was assumed, however, that this value of $E_{av.}$ should be close enough to approximate that of the sample tested for stability.

5.1c The Stability Test

As the wheat plant stands in the field, it can be approximated by a column fixed at the bottom and free at the top. The cross section of the stem, which may be treated as a hollow tube except for the nodes, changes gradually in the cross sectional dimensions as it tends to have a smaller diameter toward the top of the plant. As the plant stands in the field it carries a static load of its own stem and leaves, and an axial load represented by the head. As the plant approaches the harvesting season, the head grows heavier until it becomes the main static load acting on the stem. The plant is subjected also to the wind force, which varies in intensity from still air to very high speed wind. As the plants stand in the field, there is a great deal of shielding or mass effect which in turn reduces the wind effect. The wind forces may be approximated by a linearly distributed force with its latgest intensity towards the plant top, Figure 3.3.

For experimental convenience the stability tests were made on samples hinged from both ends, instead of fixed from one end and free in the other as it actually stands in the field. In these tests force was applied axially to the tested sample at a constant rate of deformation until the critical buckling load was reached and long enough after that in order to identify the type of buckling that took place from the shape of the resulted force deformation curve.

It should also be mentioned that most of the specimens were not perfectly straight. There was a significant initial eccentricity in the tested specimens. And as will be discussed in section 5.3, this resulted in the existence of a bending moment together with axial stress throughout the stability test.

From the shape of the resultant force-deformation curves, it was quite easy to tell whether the buckling that took place was elastic, elastic-plastic, or plastic buckling (sections 3.2, 3.3, and 3.4). Figure 5.4 shows typical elastic, elastic plastic, and plastic buckling curves resulted from the stability test.

Because the internode distance increases toward the plant top, the change in the diameter of the straw was more visible in the top portion of the plant. For this reason two samples were tested for stability from each plant. The first sample was from the lower portion of the plant where the diameter was assumed to be the

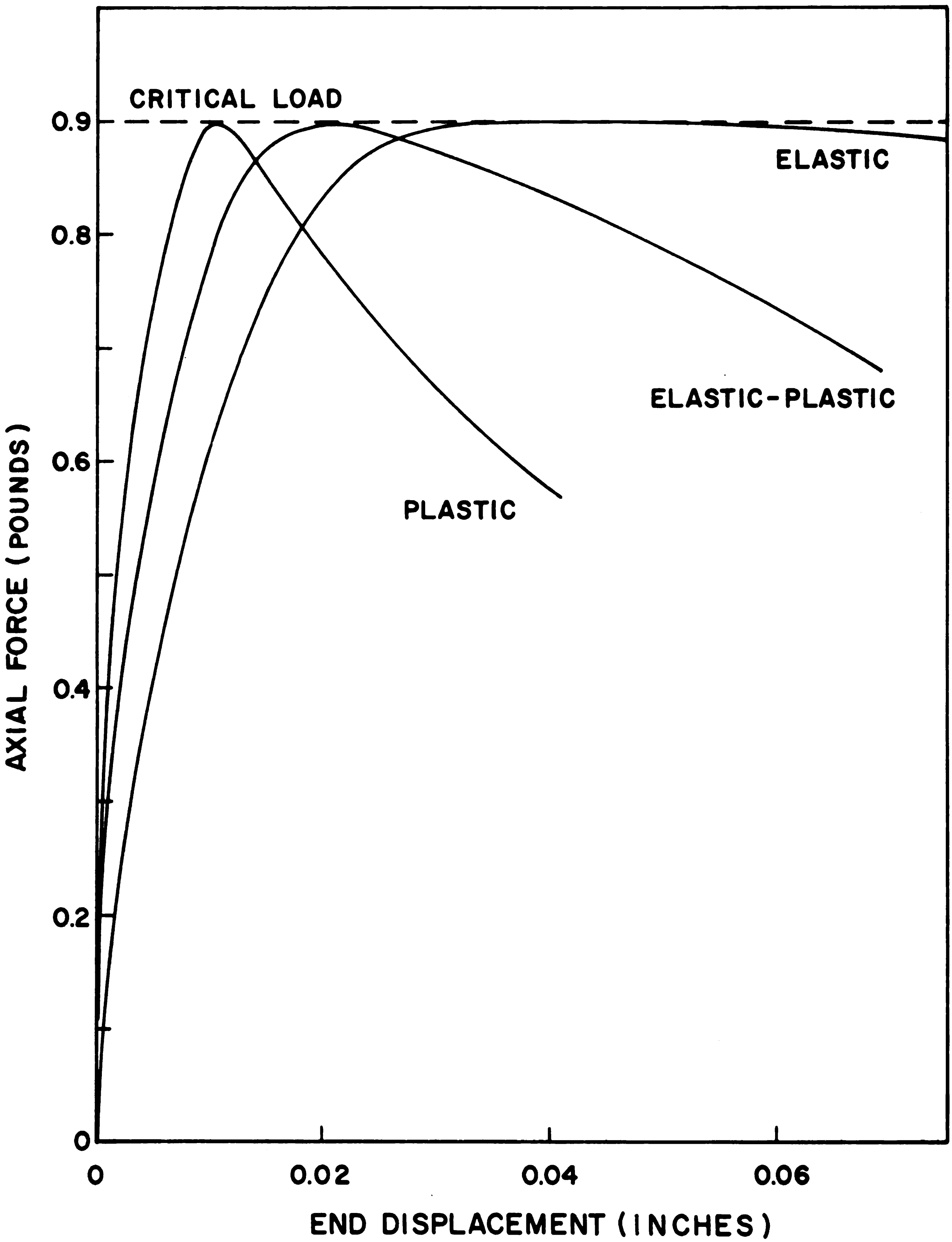

Figure 5.4--Typical elastic, elastic-plastic, and plastic buckling curves obtained from the stability tests.

same, and the second was from the top portion where the change in the diameter was obvious.

During the tests it was observed that the lateral deformation of the specimens obtained from the lower portion had the form of a sine curve. The samples obtained from the top portion, however, tended to deform more in the direction of the smaller diameter. Figures 5.5 and 5.6 show the typical deformation curves for the uniform and conical samples respectively.

5.2 Rheological Properties

The behavior of the wheat stem, being composed of structural substances and fluids, as most agricultural materials, was expected to be time dependent. The stress relaxation test showed some viscoelastic behavior in all tested specimens.

For an ideal relaxation test, it is desirable to load the specimen by means of some step-change technique, i.e., a loading which changes from zero to the desirable value within an infinitely small time interval. This technique has the advantage of minimizing the effect of stress relaxation during the loading process, but it is rather difficult to simulate experimentally. In this study the tested specimen was loaded at a constant rate of strain until a certain pre-determined level was reached, and then the deformation of the specimen was maintained

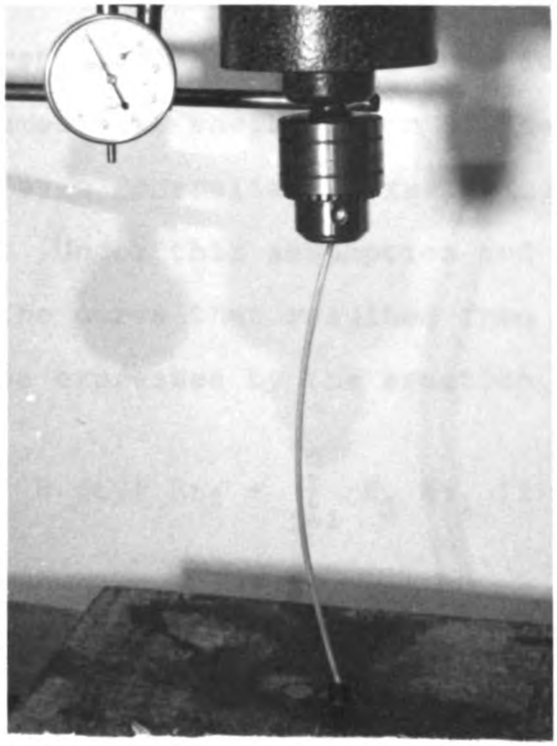

Figure 5.5--Deformation shape for straw with uniform section approximately sinusiodal.

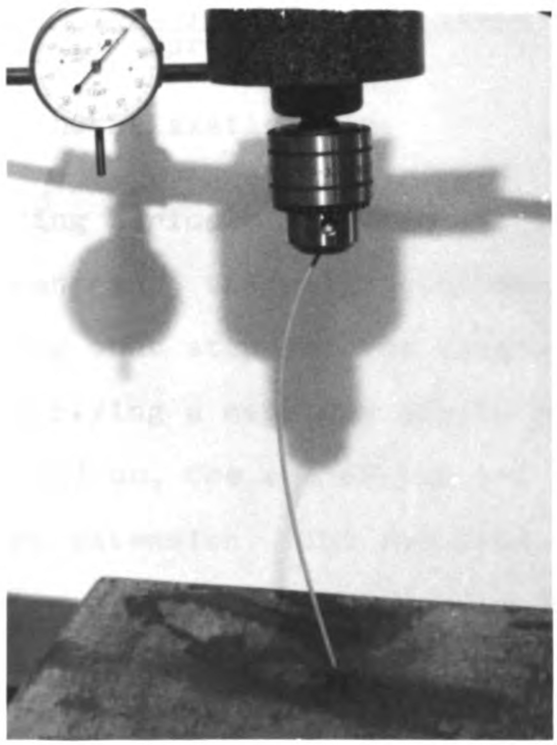

Figure 5.6--Deformation shape for straw with varying section.

constant while the force required to maintain this deformation was measured and recorded as a function of time.

It was assumed that the behavior of the wheat stem can be described by a generalized Maxwell model, Figure 3.1, section 3.1. Under this assumption and with constant strain loading, the curve that resulted from loading the wheat straw can be expressed by the equation,

$$F(t) = E_1 \int_o^t R\,dt + R\eta_2 + \sum_{i=3}^{n} E_i\,R\tau_i\,(1 - e^{-t/\tau_i})$$

$$= E_1\,R\,t + R\eta_2 + \sum_{i=3}^{n} E_i\,R\tau_i\,(1 - e^{-t/\tau_i}) \qquad (5.1)$$

where: R = the rate of strain

$$\tau_i = \frac{\eta i}{E_i} = \frac{\text{viscosity of dashpot fluid}}{\text{spring modulus}}$$

= the relaxation time

After a loading period of $t = t_1$, and then holding the displacement constant, the relaxation equation may be obtained by assuming that stopping the extension at $t = t_1$ is equivalent to applying a negative strain rate, $-R$, such that from time t_1 and on, the sum of the two opposing strains yields zero extension. The resulted expression for "F" will be

$$F(t - t_1) = E_1 R t + \eta_2 R + \sum_{i=3}^{n} E_i R\tau_i (1 - e^{-t/\tau_i})$$

$$- E_1 R(t - t_1) - \eta_2 R - \sum_{i=3}^{n} E_i R\tau_i (1 - e^{-(t-t_1)/\tau_i})$$

$$= E_1Rt_1 + \sum_{i=3}^{n} E_i R\tau_i e^{-(t - t_1)/\tau_i}(1 - e^{-t_1/\tau_i}) \tag{5.2}$$

Equation 5.2 represents the stress in the specimen being allowed to relax after loading from time, $t = 0$, to time, $t = t_1$, at a constant rate of strain, R. Equation 5.2 can be written in the form

$$F(t - t_1) = E_1Rt_1 + \sum_{i=3}^{n} F_i e^{-(t - t_1)/\tau_i} \tag{5.3}$$

where: $F_i = E_i R\tau_i (1 - e^{-t_1/\tau_i})$

= the stress in the i^{th} Maxwell element at the end of the loading process.

Figure 5.2 shows typical loading and relaxation curves obtained from compression and bending tests respectively.

By comparing the loading and relaxation equations, one can expect the following:

1. A sudden change in the encountered force at the end of the loading process can be referred to the existence of a dashpot in parallel with the spring and the Maxwell elements.

2. If the encountered force falls to zero for large values of time, then there should be no spring in parallel with other elements when a model is postulated to simulate the behavior of the tested specimen. If, on the other hand, the stress does not approach zero as time approaches infinity, and instead it tends to level up to a constant value, then obviously this type of behavior should be represented by an elastic element in parallel with the remaining elements in the generalized model.

The stress relaxation function of a Maxwell material, i.e., a material that can be represented by an element of a simple Maxwell model, is $F(t) = F_o\, e^{-t/\tau}$. This function when represented graphically on semi-log paper, will appear as a straight line with slope of $- \frac{1}{\tau}$. For models consisting of more than one simple Maxwell element in parallel, the graphical representation may be obtained by fitting several straight lines to the curve. Each straight line represents one exponential function corresponding to the relaxation of one Maxwell element. This graphical technique was introduced by Whitehead (1953) to represent the decay of electrical charges in dielectric materials.

5.2a Viscoelastic Modeling

In spite of the problems encountered in the compression test, the relaxation characteristics were studied.

The graphical technique was used to obtain the corresponding viscoelastic model. In this test it was observed that the force deformation curves showed a sudden increase in the encountered forces at the beginning of the loading process, and a sudden decrease in it at the end of the loading process and beginning of the relaxation test. And as mentioned before, this can be referred to as the existence of a dashpot in parallel with the other elements of the generalized Maxwell model. After a long relaxation time there was no sign that the relaxation curve tends to level out, and this ruled out the possibility of having an elastic element in parallel with the other elements of the model. And by using the graphical technique to study the rest of the curve, it was found that two Maxwell elements in parallel, together with the dashpot, will give a satisfactory simulation of the relaxation characteristics of the wheat straw under axial compression. Figure 5.7 shows a sample curve and the graphical technique used to chose the viscoelastic model for the relaxation of the straw under compression.

The stress-time relaxation equation of this sample takes the form

$$\sigma = \eta_1 R + \sum_{i=2}^{3} e^{-t/\tau_i}$$

This model constantly represented the relaxation behavior of the straw over the four weeks period of tests.

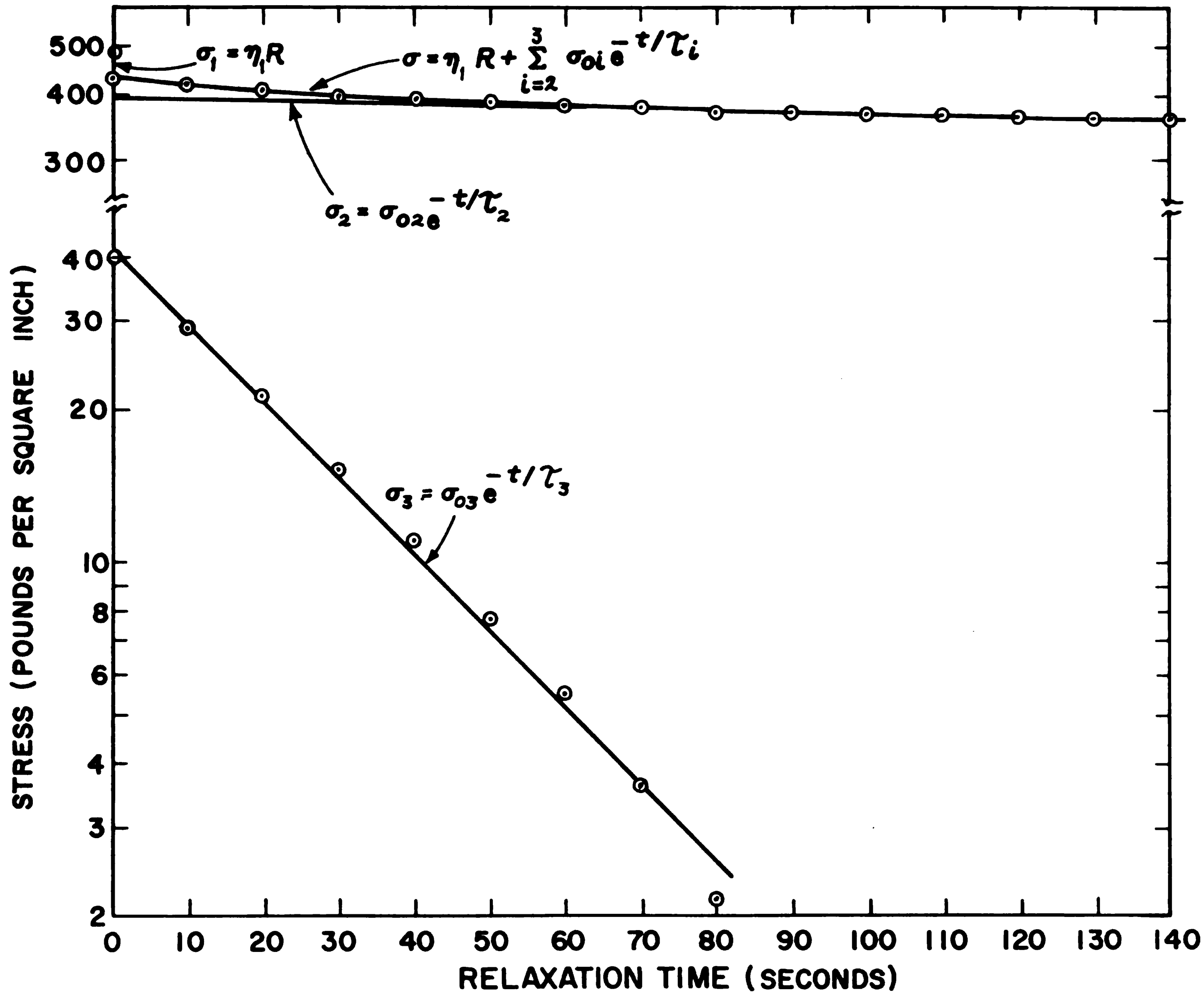

Figure 5.7--Graphical technique for evaluating the viscoelastic model parameters from the relaxation portion of the uniaxial compression test.

Appendix Table A-5 gives the values of the model parameters for the Genesee variety over the four-week period of tests.

The problems encountered in the compression tests raised some questions regarding the relaxation behavior of the tested specimens in compression. It was mainly whether the sudden change in the encountered force was a true behavior of the straw under compressive force, or due to the mounting bonds as a result of the sudden change of the rate of deformation. There is no definite answer to this statement; however, some tests of straw specimens under compression and without reinforcing the ends, showed an identical behavior. In these unmounted samples, however, the samples tended to fail at the ends because of stress concentration.

The relaxation was studied also for samples tested in bending. Neither a dashpot nor an elastic element were believed to exist in parallel with simple Maxwell elements. Using the graphical technique it was found that a model consisting of two Maxwell elements in parallel can give a good approximation of the stress relaxation of the wheat straw. This model constantly represented the relaxation behavior of the three different varieties of wheat plants throughout the four weeks period of testing. In reference to equation 5.1 and 5.3, the loading and relaxation curves were represented respectively by the following equations:

$$F(t) = E_1 R\tau_1(1 - e^{-t/\tau_1}) + E_2 R\tau_2(1 - e^{-t/\tau_2}), \quad (5.4)$$

for loading, and

$$F(t - t_1) = F_1 e^{-(t - t_1)/\tau_1} + F_2\, e^{-(t - t_1)/\tau_2},$$

for relaxation, where:

$$F_i = E_i\, R\tau_i\, (1 - e^{-t_1/\tau_i})$$

R = the rate of deformation of the center of the tested specimen

$$\tau_i = \frac{\eta_i}{E_i}$$

t_1 = the time at which the loading was ended and relaxation test was started.

Figure 5.8 shows a sample of a relaxation curve and the graphical technique used to find the viscoelastic model for the bending. Appendix Table A-6 gives the values of τ_1, τ_2 and F_1, F_2 obtained from the bending test for the three wheat varieties, Comanche, Redcoat and Genesee, for the four weeks of tests.

5.2b Evaluation of the Modulus of Elasticity from the Loading Curve

It was mentioned in section 5.1 that the modulus of elasticity was evaluated from the slope of the tangent of the starting portion of the loading curve. In both tension and compression curves the slope gave the force-deformation ratio which was used together with informations of the cross-sectional area and sample length to evaluate E as:

$$E = \frac{\text{Force}}{\text{Area}} \times \frac{\text{original length}}{\text{deformation}}\ .$$

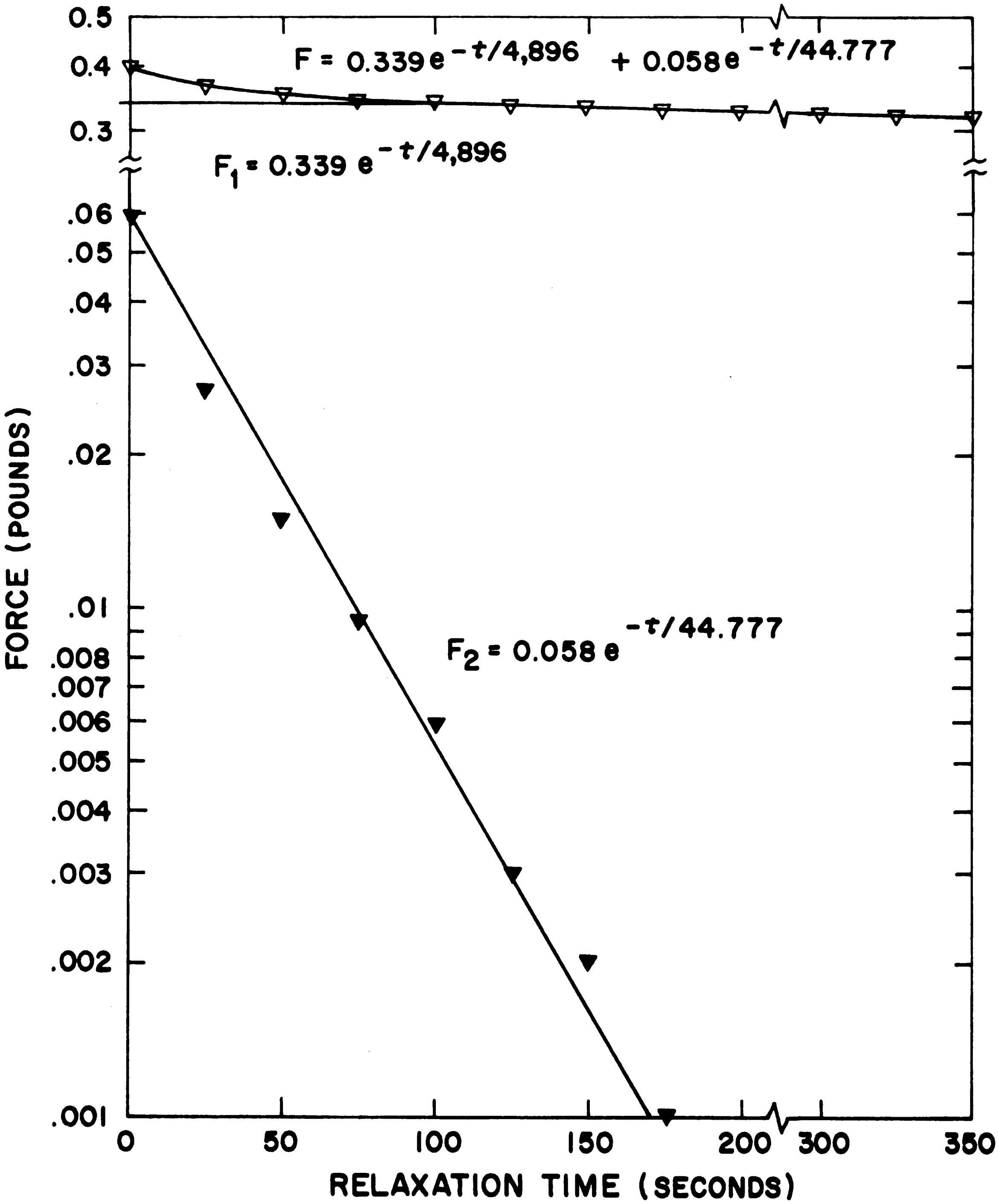

Figure 5.8--A sample of the relaxation curve and the graphical technique for evaluating the viscoelastic parameters from the bending test.

Similarly the force, F, and deformation, y, of the middle point of the straw tested in simple bending were used together with the moment of inertia of the cross section, I, and length of the span, L, to evaluate E from the relation

$$E = \frac{F\ L^3}{48\ I\ Y}\ .$$

Theoretically if we refer to the function representing the loading curve in bending:

$$F(t) = E_1R\tau_1\left[1-e^{-t/\tau_1}\right] + E_2R\tau_2\left[1-e^{-t/\tau_2}\right]$$

$$= E_1R\tau_1\left[1-(1-\frac{t}{\tau_1} + \frac{t^2}{(2!)\tau_1{}^2} - \frac{t^3}{(3!)\tau_1{}^3} + ..)\right]$$

$$+ E_2R\tau_2\left[1-(1-\frac{t}{\tau_2} + \frac{t^2}{(2!)\tau_2{}^2} - \frac{t^3}{(3!)\tau_2{}^3} + ...)\right]$$

$$= E_1R\left[t - \frac{t^2}{(2!)\tau_1} + \frac{t^3}{(3!)\tau_1{}^2} - ..\right]$$

$$+ E_2R\left[t - \frac{t^2}{(2!)\tau_2} + \frac{t^3}{(3!)\tau_2{}^2} - ...\right] \qquad (5.6)$$

and

$$F'(t) = E_1R\left[1 - \frac{t}{\tau_1} + \frac{t^2}{(2!)\tau_1^2} - \ldots\right]$$

$$+ E_2R\left[1 - \frac{t}{\tau_2} + \frac{t^2}{(2!)\tau_2^2} - \ldots\right]$$

from which

$$\lim_{t \to o} F'(t) = E_1R + E_2R \qquad (5.7)$$

which represents the effect of the elastic elements only, and completely independent of the damping effect in the specimen.

If we follow the same procedure for the function representing the loading curve in compression we will end with an expression identical to equation 5.7.

5.2c The Maturity Effect on the Viscoelastic Behavior

As shown in Figure 5.9, the relaxation time tends to increase as the straw becomes more mature. This change with time was more significant early in the harvesting season, i.e., during the first two weeks of testing. For the same period the moisture content (wet basis) and the linear density of the wheat plants decreased as shown in Figure 5.1. And as $\tau = \frac{\eta}{E}$, one can conclude that in order for τ to increase one of three possibilities must exist; either E decreases while η remains approximately constant, or η increases at higher rate than E, or η increases while

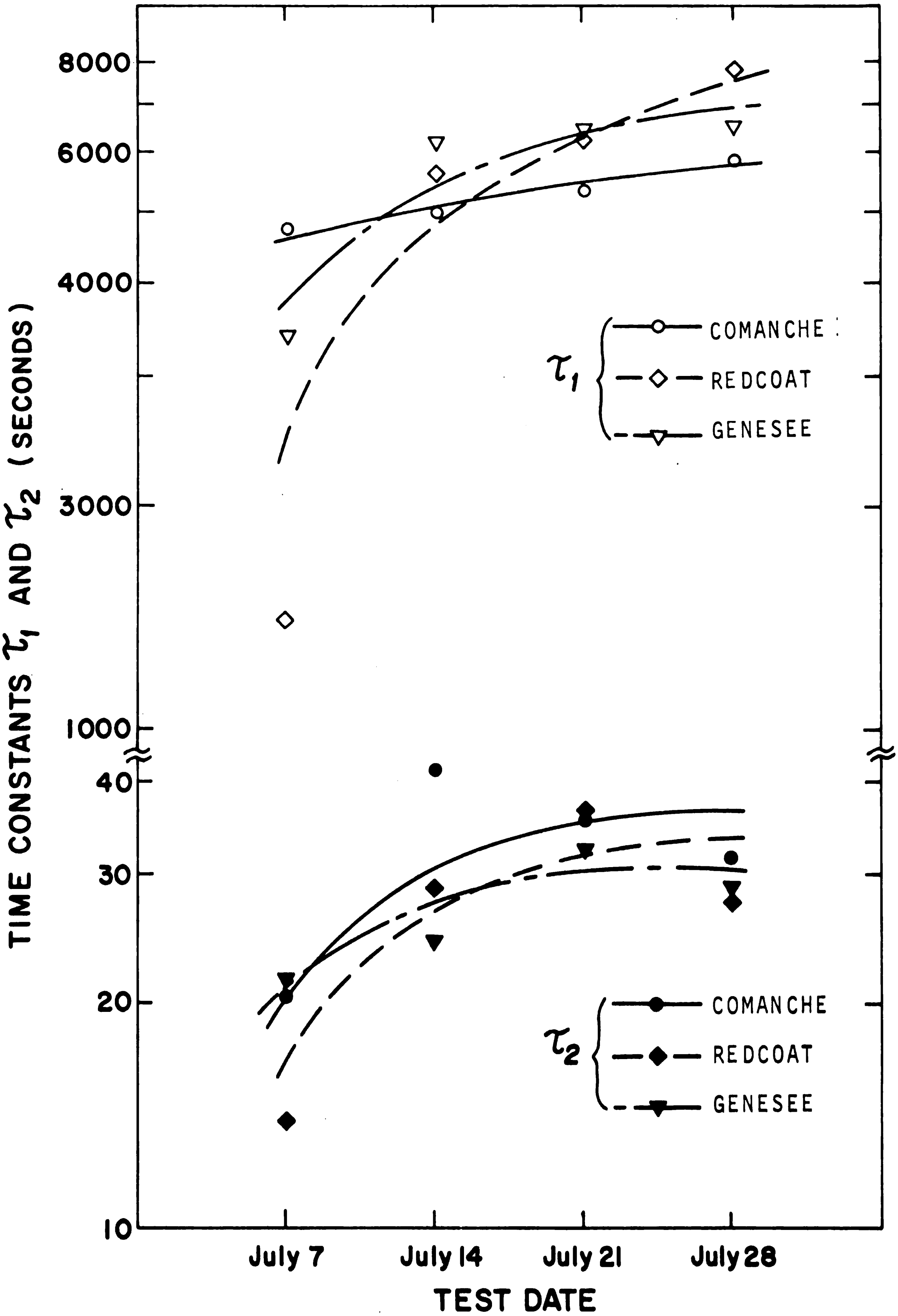

Figure 5.9--Variation of viscoelastic parameters with maturity obtained from the relaxation of samples in bending.

E remains approximately constant. From the data of E listed in Appendix Table A-4 one can say that the last of the three mentioned possibilities is more likely to take place. If this is the case, this means that η becomes higher with maturity which means that the dashpots become stiffer with maturity. Physically if we imagine a hypothecal situation in which the damping factor became infinitely high, a simple Maxwell model will become similar to an elastic element in series with a rigid body, i.e., the simple Maxwell model will behave simply like an elastic element. Theoretically this proves to be true as we consider equation 5.6 which represents the loading function for two simple Maxwell models in parallel:

$$F(t) = E_1 R \left[t - \frac{t^2}{(2!)\tau_1} \quad \frac{t^3}{(3!)\tau_1{}^2} - \ldots \right]$$

$$+ E_2 R \left[t - \frac{t^2}{(2!)\tau_2} + \frac{t^3}{(3!)\tau_2{}^2} - \ldots \right]$$

$$\lim_{(\tau_1, \tau_2) \to \infty} F(t) = R\, t\, (E_1 + E_2) \tag{5.8}$$

This concludes that the ultimate case is an elastic material.

For the wheat plant one can conclude that as the plant becomes more mature, the viscous effect becomes lower and the plant tends to behave more like an elastic material.

5.3 The Stability of the Plant

While the engineers have devoted considerable attention to the buckling stability of metallic structures, they have done little to investigate how nature handled this problem. Agricultural engineers are now investigating biological structures with the same degree of mathematical sophistication and instruments previously used on engineering materials. Theories of plant structure and data accumulated can be of great importance for more understanding and better communication between the engineer and the plant scientists. It has been a custom for the engineer to try to think of a way to treat or harvest a plant no matter how peculiar the existing shape of the plant might be. If the day comes in which the engineer reaches the stage of understanding the nature of this biological structure in the same way he understands common engineering materials, he probably can ask the plant scientist to look for a certain property or variety that has certain characteristics which if achieved can enable him to make a break-through in the technology and efficiency of his machine.

An example for that was the process of developing standing harvestors which were supposed to strip the grains from the plant as it stands in the field. If such a machine proved successful it could provide a very efficient way of harvesting with a smaller and more economical machine. Theoretically such a function could be achieved if we have the plant standing straight with the head at the very top. Once the stability of the plant is clearly understood, the plant scientists can look for certain varieties which can achieve these requirements on stability. He can even specify certain properties in the stem of the plant, its shape and strength which might achieve such requirements. In this case while the plant scientist is looking for a better yield and certain other qualities in the grains, he can also look for the physical structure which will satisfy the requirements of the engineer.

In this investigation of the stability of the plant structure, the intention was to explore the means of handling such a study. Unfortunately, most of what is available in literature deals with metal structures which were designed from materials, with known behavior, to perform certain functions. A good number of this information deals with idealized shapes and structures which are not common in biological structures.

In order to establish some basis for this study, an idealized plant structure was assumed. After that some modifications of the originally assumed shape took place in order to have a situation closer to reality. These modifications were made on separate steps to reduce the complexity of the problem. One should also take in consideration the fact that this study is by no means a complete one, it is rather a start for more work to follow in the future.

As a start, a specimen of the wheat plant stem was assumed to have buckling strength similar to that of an elastic, straight hollow tube which was made of a material whose modulus of elasticity is equal to that of the plant stem. The values of the modulus of elasticity were those obtained from the bending test and listed in Appendix Table A-4. The tests were made on three varieties of wheat plants, Comanche, Redcoat and Genesee. Two samples were tested from each plant, one from the lower part and the other from the top. The tested samples were hinged from both ends. Because the moduli of elasticity used were the average of three tests, different plant and due to the variation from one plant to another, it was realized that these average values of E may not necessarily be the exact values of E for the samples being tested for buckling stability. The theoretical values for the samples from the lower portion were calculated from the equation

$$P_{cr} = \frac{\pi^2 E\ I}{L^2} \quad ,$$

where: E = Modulus of elasticity obtained from the bending test.

I = Moment of inertia of the cross section which was assumed to be constant for samples from the lower part of the plant.

L = Sample length.

Appendix Table A-7 shows the values of the theoretical and experimental values of P_{cr} for the samples from the lower part of the plant over the four-weeks period of tests. In each test the type of buckling, elastic, elastic-plastic, or plastic, was identified from the shape of the force-deformation curve obtained from testing each sample.

The factors which contributed to the variations between the theoretical and experimental values, other than E, were the initial shape and the inelastic behavior of the straw. Other factors influencing the stability of the plant as it stands in the field include also the wind forces, and the influence of cross-sectional variation along the plant. Each one of these three major factors will be discussed separately.

5.3a The Effect of the Initial Shape and Inelastic Behavior

As mentioned in section 5.1c, the tested specimens were not straight. They had some initial eccentricity which may be approximated to a sine curve. In section 3.2b the stability of an elastic column with initial eccentricity of this type was discussed. Also, it was found, in section 3.2b, that if we assume small deformations and as long as we stay in the elastic range, the critical load will be the same as that for straight column. The initial curvature, however, will result in a larger deformation.

For the case of wheat straw which does not behave like a perfectly elastic material, the situation is different. In fact, we have two factors working together in order to increase the deformation and deviate from the elastic behavior before reaching the critical load: (i) the damping factor which allows the material to relax while the load is being applied at a constant rate of deformation, and therefore result in a larger deformation for the same load; (ii) the elastic elements in the material had the tendency to have a plastic like behavior for large deformations. And since bending and direct stress occur simultaneously from the beginning and grow together with increasing the axial load, P, no strain reversal is presumed to occur on the concave side of the deflected specimen at the instant at which the critical load is reached. When P is increased until the proportional limit is exceeded in the entire cross section, or at least in the highest stressed portion of the cross section, plastic flow is presumed to take place. In this case, we will have the situation discussed in section 3.4, where, as in Figure 3.9, the resulted value of the critical load will be lower than the one obtained from both the theory of elastic stability and the tangent modulus theory of inelastic buckling.

After the load, P, is removed, the sample returns toward its originally straight form but retains a slightly bent shape owing to the residual plastic strain in those fibers where the proportional limit was exceeded. And as was shown in Figure 5.4, section 5.1, there are three possible situations depending on the extent to which the elastic limit was exceeded: (i) If we are still within the elastic range and the proportional limit, if there is one. This was referred to as elastic buckling. The experimental values should be the closest to the values obtained theoretically from the theory of elasticity. (ii) Outside the proportional and not far from the elastic range; and in this case we will have an elastic and some plastic buckling which may have some non-recoverable strain in the highest stressed portion of the section. This situation was referred to in this thesis as the transition or "elastic-plastic" buckling. (iii) Outside both the proportional limit and the elastic range. This is referred to as "plastic" buckling.

The situation, where plastic flow takes place in the section where the elastic range was exceeded, could also be considered analogous to the double-modulus model of plastic buckling. A successful compression test may enable checking the validity of this assumption.

5.3b The Influence of the Lateral Forces

The principal source of lateral forces is the wind. If we have a single plant standing alone in the field, the wind forces may be approximated by a uniformly distributed force. However, the fact that the plants provide shielding to each other, reduces the intensity of these forces.

A linearly distributed horizontal force with its largest magnitude acting toward the head of the plant may be a logical approximation of the wind forces. The intensity of these forces (especially q(x) Figure 3.3) depend mainly on the wind speed and air relative humidity.

As demonstrated in section 3.2c, the displacement of the straw is greatly influenced by the intensity of the wind forces. A strong wind will result in a very large deformation of the straw and therefore a large moment acting on it because of the axial force, mainly the plant head. As a result, the stresses in some sections might exceed the proportional and elastic ranges, and the final result will be plastic and non-recoverable deformations in the straw.

5.3c The Effect of the Cross-Sectional Variation

As mentioned in section 5.1c, the gradual decrease in the cross-sectional dimensions toward the top of the plant can be assumed linear. The direct effect of such change will be a reduction in the axial force that is required to cause buckling.

The theoretical treatment of this effect was made in detail in section 3.2d. For the plant as a whole, fixed from one end where the largest cross section exists and free from the other, the critical load will be:

$$P = \mu \frac{\pi^2 E_t I_m}{4 L^2}$$

where: E_t = the tangent modulus of elasticity for this stress level.

I_m = The moment of inertia of the large section.

L = The plant height.

$$\mu = \frac{1 + 4 K_1^2}{\pi^2} \left(1 - \frac{h_o}{h_m}\right)^2 .$$

This is identical to the solution for columns with uniform sections except for the factor μ. Figure 5.10 shows the values of μ, for this case of "symmetrical column with straight chords" plotted as a function of the ratio between the smallest dimension to the largest (i.e., $\frac{h_o}{h_m}$).

The value of μ is always smaller than one. Hence, the change in the cross section results in smaller critical loads.

In the experimental tests, to check the effect of the change in the cross section, the samples were hinged from both ends. For this situation of a "nonsymmetrical column with straight chords," the theoretical solution of section 3.2d resulted in a critical buckling load equal to

$$P = \mu \frac{\pi^2 E_t I_m}{L^2} ,$$

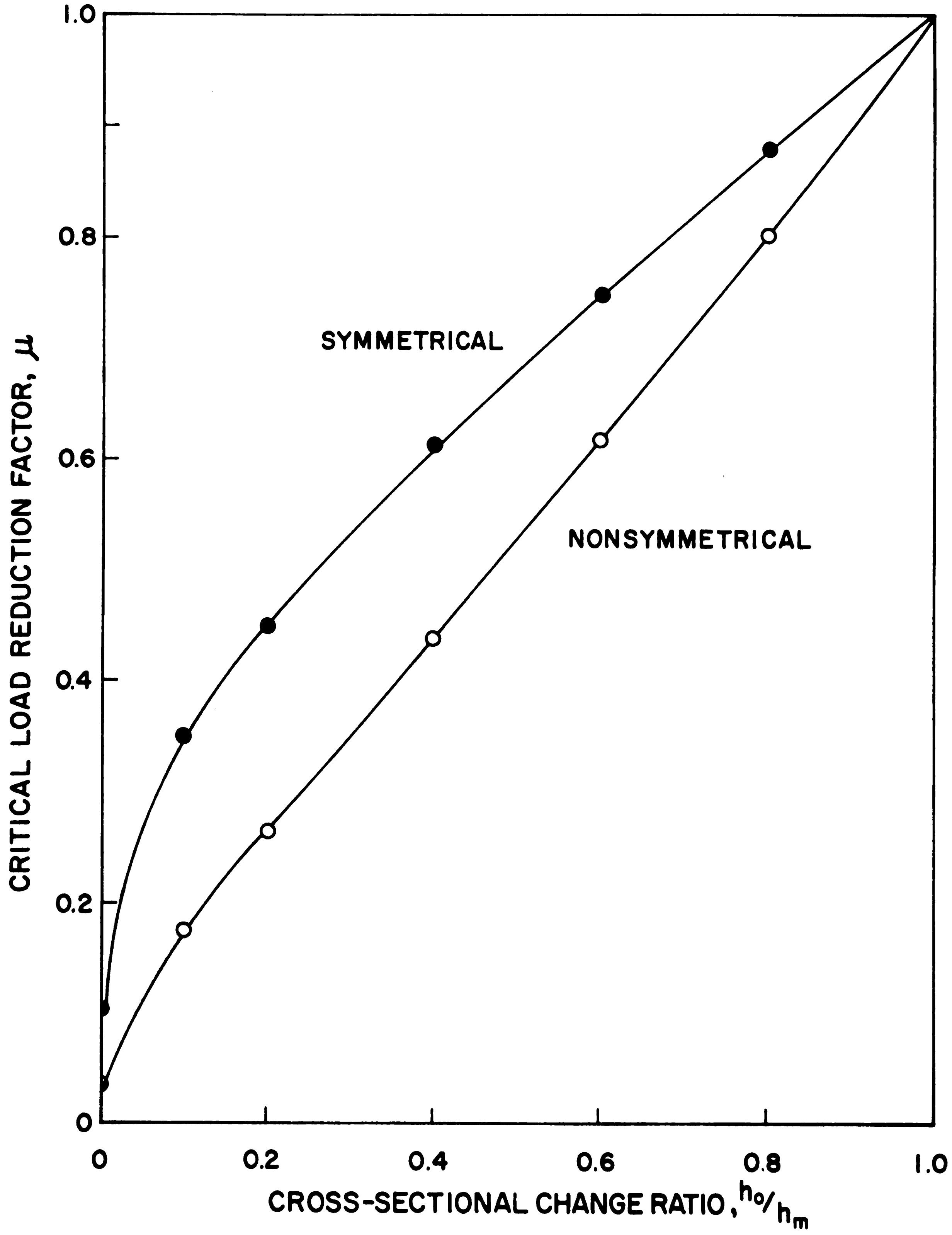

Figure 5.10--The values of the factor μ as a function of the change in the cross section (i.e. h_o/h_m).

and for this situation

$$\mu = \tfrac{1}{4}\left(1 - \frac{h_o}{h_m}\right)^2 \left[\frac{1}{\pi^2} + \frac{4}{(\log_e h_o - \log_e h_m)^2}\right] .$$

For this "nonsymmetrical column with straight chords," the values of μ are shown in Figure 5.10, plotted as a function of $\frac{h_o}{h_m}$. For this case, also, μ is always less than one. Therefore the cross-sectional reduction will always result in a reduction in the critical buckling load.

The experimental and theoretical values of the critical buckling loads for the tested specimens are shown in Appendix Table A-8. In this data, the experimental values are frequently smaller than the ones predicted theoretically. The principal reason for this was the large initial deflection in all the specimens tested. This large initial deflection resulted in a large bending moment acting from the beginning of the loading process and increasing as the applied load increases.

5.4 The Influence of the Plant Physical Changes on Its Strength and Behavior

From the collected information thus far, it is possible to visualize the general behavior of the plant and the effect of the physical changes that take place as the plant becomes more mature.

Early in the growing season the plant has a very high moisture content and therefore high viscous properties.

The weight of the plant head is much smaller, compared with its weight later during the harvest season. In this stage the plant is very stable and less sensitive to plastic deformations due to the lateral forces resulting from the wind. This is mainly because of the viscous effect which enables the plant to recover its original shape even after large deformations.

As the plant becomes more mature, the viscous behavior becomes less, and the plant head grows heavier. In this stage the plant becomes more sensitive to plastic strains. Such strains take place as a result of the combined effect of the axial force, provided by the plant head, and the lateral force, resulted from the wind forces.

One should also emphasize two facts: the first is that plant head weight is less than the critical buckling load of the plant as a whole, and the second is that the presence of the nodes, which varies in number between three to six, provides an additional inertia and stiffness to the plant stem. These two factors help the plant to remain stable. On the other hand the length and small diameter of the upper internode tend to reduce the buckling strength. The exposure to wind and sun radiation reduces the moisture content of the upper internode which further weakens it.

Considering these factors, one can conclude that for the same intensity of wind the plant has a better chance to recover its original stable shape early in the growing season compared with that during the harvesting season. In some cases the wind together with the head weight caused a situation of instability such that the stresses in the plant do not exceed the elastic range except the top internode, which is the weakest. In such a situation the plant as a whole may be able to recover its original shape except for the top part which retains a slightly bent shape owing to the residual plastic strains in those fibers where the elastic limit was exceeded. As the same process is repeated, the deformations get even larger because of the initial eccentricity that was a result of the first plastic instability in the top part. Successive processes of that nature results in the shape that the plants actually have during the harvesting season. In such stages the plant stem is more sensitive to complete failure with high speed wind because of the larger bending moments introduced as a result of the deformed shape of the plant.

6. SUMMARY

This study was initiated to study the behavior of the cereal grain plant under applied stresses. Since the plant stem is the principal supporter of the plant structure, the understanding of its behavior and physical properties is of major importance to the engineer. The mechanical and rheological properties of the plant stem as well as the stability of the plant structure were investigated. Tests were conducted over a period of four weeks to study the maturity effect, and were limited to three varieties of wheat--(Triticum Vulgarus)--Comanche, Redcoat and Genesee.

All tests were conducted in a testing chamber under controlled temperature and humidity conditions. Tension, compression, and bending tests were conducted to study the behavior of the straw to applied stresses. Elastic and viscous properties of the straw were evaluated using elastic and viscoelastic flexure theory. The buckling stability was studied for the plant structure.

Theoretical equations were derived for the evaluation of the elastic and viscoelastic moduli from quasi-static flexure. Critical load and deformation equations were derived from the theory of elastic stability.

The wheat plant reacted to applied forces as an elastic-plastic-viscous body. A viscoelastic model, consisting of one viscous and two simple Maxwell elements in parallel, simulated the behavior of the plant stem in compression. The stem behaved in flexure similar to two simple Maxwell elements in parallel.

The stability of the plant structure was explained by employing the theory of elastic stability together with the concepts of inelastic buckling. The existence of the nodes provided a localized increase in the inertia of the straw which contributed to the stability of the plant. The decrease in the outside diameter of the plant stem toward the plant top was assumed linear and the wall thickness constant. This cross-sectional change reduced the buckling strength of the plant by a factor which is a function of the rate of change in the cross section. The top internode, which is the longest, was the least stable. Wind force acting on the plant, as it stands in the field, was approximated by a linearly distributed horizontal force having its largest magnitude at the top of the plant. These forces greatly influenced the deformation of the plant.

As the plant reached the harvesting stage, the viscous properties decreased and the elastic properties dominated the behavior of the plant for small deformations. In this stage the head weight becomes the principal axial force acting on the plant. A high velocity wind will force the plant to deform from its initial straight shape. The strains in the top internode may exceed the elastic range. As the wind stops the plant tends to recover its original shape but retains a slightly curved shape due to the residual plastic strains in the fibers where the elastic limit was exceeded. Successive wind forces together with the growth of the plant head increase the residual plastic strain result in the familiar bent shape of the top internode during the harvesting season. An exceptionally high intensity wind, in this stage, may result in the failure or lodging of the plant.

7. CONCLUSIONS

1. The wheat plant reacted as an elastic-plastic-viscous body to applied forces.
2. A viscoelastic model consisting of one viscous and two simple Maxwell elements in parallel simulated the behavior of the plant stem in compression.
3. The plant stem behaved in flexure similar to two simple Maxwell elements in parallel.
4. The stability of the wheat plant structure was explained by employing the theory of elastic stability together with the concepts of inelastic buckling.
5. The existence of nodes increased the buckling strength while the decrease in the cross-sectional area towards the plant top decreased it.
6. The top internode, being the longest and smallest in cross-sectional area, is least stable and more sensitive to plastic deformations.
7. The wind force was approximated by a linearly distributed horizontal force having its largest

magnitude at the top of the plant. These forces greatly influence the deformations of the plant.

8. The viscous properties decreased with maturity, and the elastic properties dominated the behavior of the stem for small deformations.

9. High speed winds resulted in large deformations, especially in the top internode. If the strains exceed the elastic range, plastic flow takes place, and the plant retains a slightly bent shape. Successive wind forces, together with the growth in weight of the plant head, results in a familiar bent shape of the top internode during the harvesting season. An exceptionally high speed wind, in this stage, may result in failure, or lodging of the plant.

8. RECOMMENDATIONS FOR FUTURE WORK

The results of this investigation indicate the need for additional work in the following areas:

1. Refining the optical strain measurement technique and using it to obtain true stress-strain curves for tension and compression. Then using these curves to check the theoretical analysis of the stability of the inelastic curved beam presented in section 3.4.
2. Studying the variation of the plant parameters from one plant to another and employing statistical analysis to study such variation and its distribution.
3. Extending the maturity study to start early in the growing season.
4. Studying the behavior of the plant under dynamic loading.
5. Studying the structure of the head. The kernal support strength and orientation should also be studied under static and dynamic loading.

REFERENCES

Bland, D. R.
1960 The Theory of Linear Viscoelasticity. Pergamon Press, New York, N. Y.

Bleich, Friedrich
1951 Buckling Strength of Metal Structures. McGraw-Hill Book Company, Inc., New York, N. Y.

Burmistrova, M. F. and others.
1956 Fiziko-mekhanicheskie svoistva sel'skokhozy aistvennykh rastenii. Gosudarstvennoe izdatel'stvo, sel'skokhozyaistvennoi literatury, Moskva. English translation is published by the National Science Foundation entitled "Physicomechanical Properties of Agricultural Crops." Available from the Office of Technical Services, U. S. Department of Commerce, Washington 25, D. C.

Crandall, S. H.
1959 An Introduction to the Mechanics of Solids. McGraw-Hill Book Company, Inc. New York, N. Y.

Diener, R. G.
1965 Some Mechanical Properties of Cherry Bark and Wood. Unpublished Ph.D. Thesis, Michigan State University, East Lansing, Michigan

Esau, Katherine
1965 Plant Anatomy. John Wiley and Sons, Inc., New York, N. Y.

Finney, E. E., C. W. Hall and G. E. Mase
1964 Theory of Linear Viscoelasticity Applied to the Potato. Journal of Agricultural Engineering Research 9(4):307-312.

Frey-Wyssling, Albert
1952 Deformation and Flow in Biological Systems. Interscience Publishers, Inc., New York, N. Y.

Halyk, R. M. and L. W. Hurlbut
1964 Tensile and Shear Strength Characteristics of Alfalfa Stems. ASAE Paper No. 64-817 presented at Winter Meeting of ASAE, New Orleans, Louisiana.

Jastrzebski, Z. D.
1964 Nature and Properties of Engineering Materials. John Wiley and Sons, Inc., New York, N. Y.

Kollman, Von Franz
1964 Uber die Beziehungen Zwischen rheologischen und Sorption-Eigenschaften (am Beispiel von Holz). Rheologica Acta, Band 3, Heft 4.

McClelland, R. H. and R. E. Spielrein
1957 An Investigation of the Ultimate Bending Strength of Some Common Pasture Plants. Journal of Agricultural Engineering Research, Volume 2. The British Society for Research in Agricultural Engineering.

Meyer, K. H.
1950 Natural and Synthetic High Polymers. Interscience Publishers, Inc., New York, N. Y.

Mohsenin, N. N., H. E. Cooper and L. D. Tukey
1963 An Engineering Approach to Evaluating Textural Factors in Fruits and Vegetables. ASAE Transactions 6(2):35-38, 92.

Morrow, C. T.
1965 Viscoelasticity in a Selected Agricultural Product. Unpublished M. S. Thesis, The Pennsylvania State University.

Morrow, C. T. and N. N. Mohsenin
1965 Consideration of Agricultural Products as Viscoelastic Bodies, ASAE Paper No. 65-810 presented at Winter Meeting of ASAE, Chicago, Illinois.

Percival, J.
1921 The Wheat Plant. E. P. Dutton and Company, New York, N. Y.

Shpolyanskaya, A. L.
1952 Structural and Mechanical Properties of the Wheat Grain. Colloid Journal (U.S.S.R.), 14(1):137-148

Suggs, C. W. and W. E. Splinter
1964 Mechanical Properties of Tobacco Stalks. ASAE Paper No. 64-801 presented at Winter Meeting of ASAE, New Orleans, Louisiana.

Timbers, G. E.
1964 Some Mechanical and Rheological Properties of the Netted Gem Potato. M. S. Thesis, University of British Colombia.

Timoshenko, S. P. and J. M. Gere
1961 Theory of Elastic Stability. McGraw-Hill Book Company, Inc. New York, N. Y.

Zoerb, G. C.
1958 Mechanical and Rheological Properties of Grain. Unpublished Ph.D. Thesis, Michigan State University, East Lansing, Michigan.

APPENDIX

TABLE A-1.--Modulus of elasticity ($lb/in^2 x 10^{-3}$) obtained from tension test.

Test Date	Comanche[1]		Redcoat[1]		Genesee[1]	
	Upper[2]	Lower[2]	Upper	Lower	Upper	Lower
7/14/65	213	335	273	312	220	210
	260	264	245	287	162	165
	244	242	213	225	244	290
7/21/65	217	262	239	254	187	246
	197	291	281	312	264	309
	162	253	326	293	270	342
7/28/65	262	354	215	218	242	219
	185	313	380	327	312	372
	272	317	308	363	314	357

[1]Variety.

[2]Specimen taken from upper or lower part of the plant.

TABLE A-2.--Modulus of elasticity ($lb/in^2 x 10^{-3}$) obtained from compression test.

Test Date	Comanche[1]		Redcoat[1]		Genesee[1]	
	Upper[2]	Lower[2]	Upper	Lower	Upper	Lower
7/7/65	169	320	254	290	202	200
	195	198	172	161	219	198
	127	228	201	196	231	201
7/14/65	270	181	184	172	345	176
	227	160	138	147	170	180
7/21/65	168	156	232	300	154	294
	141	159	267	203	212	169
	324	258	252	231	206	202
7/28/65	129	174	197	159	336	276
	178	184	284	313	367	229
	240	321	184	188	239	301

[1]Variety.

[2]Specimen taken from upper or lower part of the plant.

TABLE A-3.--Data for loading curve (compression) using optical strain measurement technique.

Sample Number	Photo Number	Measured Length, in	Actual Length, in	Strain, in	Cross Sec. Area, in^2	Force, lb	Stress, lb/in^2
1	1	37.88	0.5000	0	0.00457	1.70	371
	2	37.78	0.4986	0.0024		5.44	1,189
	3	37.76	0.4984	0.0032		7.66	1,675
2	4	39.46	0.5000	0	0.00584	0	0
	5	39.44	0.4997	0.0005		0.40	68
	6	39.43	0.4996	0.0076		1.50	256
	7	39.38	0.4990	0.0020		4.10	701
	8	39.34	0.4985	0.0030		6.40	1,094
	9	39.30	0.4980	0.0041		8.58	1,467
	10	39.30	0.4980	0.0041		8.64	1,477
3	11	39.10	0.5000	0	0.00470	0	0
	12	39.06	0.4995	0.0010		2.37	505
	13	39.04	0.4992	0.0015		3.72	792
	14	39.03	0.4991	0.0018		3.90	830
	15	39.00	0.4987	0.0026		5.12	1,090
	16	39.00	0.4987	0.0026		4.66	992

TABLE A-4.--Modulus of elasticity ($lb/in^2 x 10^{-3}$) evaluated from the bending test.[1]

Test Date	Comanche[2]	Redcoat[2]	Genesee[2]
7/7/65	785	1,107	827
	1,133	1,315	763
	1,678	990	800
7/14/65	856	759	834
	951	752	780
	720	814	706
7/21/65	709	1,054	1,198
	629	1,014	659
	640	859	1,028
7/28/65	885	1,061	859
	787	758	923
	695	694	845

[1]The lower portion of the plant.

[2]Variety

TABLE A-5.--Viscoelastic model parameters obtained from the compression test for the wheat variety: Genesee.

Test Date	Sample Number	Top Portion Sample			Lower Portion Sample		
		η[1]	τ_1, sec	τ_2, sec	η[1]	τ_1, sec	τ_2, sec
7/7/65	1	23.738	2,062	22.87	17.951	1,388	26.20
	2	20.511	2,104	21.32	18.312	1,734	20.34
	3	17.705	1,969	20.59	16.893	820	16.84
7/14/65	1	32.362	1,132	23.09	29.898	1,043	18.79
	2	35.794	1,674	20.55	34.387	1,587	24.57
	3	25.812	1,421	21.40	30.231	1,054	17.45
7/21/65	1	40.359	734	13.82	64.624	1,280	29.03
	2	55.601	1,142	14.15	41.795	1,068	23.33
	3	36.194	817	25.20	51.056	1,239	29.12
7/28/65	1	64.256	2,085	44.55	54.545	978	33.67
	2	64.281	2,184	27.88	55.716	1,032	27.39
	3	65.856	1,456	19.63	57.527	1,223	22.05

[1]The units of η are (lb sec/in^3) x 10^{-4}.

TABLE A-6.--Viscoelastic model parameters F_1, τ_1 and F_2, τ_2 obtained from the relaxation curves of the bending test.

Test Number	Date	Sample Number	F_1, lb	τ_1, sec	Average τ_1 sec	F_2, lb	τ_2, sec	Average τ_2 sec
				Comanche[1]				
1st Test	7/7/65	1	0.281	3,840	4,763	0.009	22.755	20.348
		2	0.248	4,300		0.004	15.533	
		3	0.332	6,150		0.009	22.755	
2nd Test	7/14/65	1	0.420	4,838	5,031	0.052	38.365	41.491
		2	0.339	4,896		0.006	44.777	
		3	0.595	5,360		0.069	41.330	
3rd Test	7/21/65	1	0.308	6,641	5,372	0.020	36.067	35.365
		2	0.278	4,219		0.019	33.962	
		3	0.305	5,256		0.008	36.067	
4th Test	7/28/65	1	0.508	5,646	5,869	0.024	37.050	31.361
		2	0.778	6,821		0.042	28.419	
		3	0.655	5,139		0.055	28.614	
				Redcoat[1]				
1st Test	7/7/65	1	0.802	1,215	1,417	0.034	14.175	13.960
		2	0.700	1,619		0.038	13.745	
2nd Test	7/14/65	1	0.568	7,185	5,630	0.028	28.419	28.685
		2	0.198	4,178		0.009	22.755	
		3	0.914	5,527		0.072	34.881	

3rd Test	7/21/65	1	0.550	6,763	6,361	0.048	32.289	36.555
		2	0.572	6,374		0.050	38.833	
		3	1.020	5,945		0.098	38.542	
4th Test	7/28/65	1	1.252	9,358	7,871	0.042	26.754	27.543
		2	0.316	4,930		0.014	25.694	
		3	0.293	9,325		0.024	30.182	
				Genesee[1]				
1st Test	7/7/65	1	0.659	3,631	3,404	0.030	19.957	21.965
		2	0.410	2,720		0.008	18.033	
		3	0.704	3,861		0.006	27.905	
2nd Test	7/14/65	1	0.765	6,045	6,212	0.050	24.136	24.107
		2	0.885	7,026		0.050	22,638	
		3	0.648	5,566		0.040	25.547	
3rd Test	7/21/65	1	0.997	7,874	6,497	0.029	18.697	32.128
		2	0.626	5,680		0.060	36,635	
		3	0.972	5,937		0.142	41.053	
4th Test	7/28/65	1	0.857	7,263	6,513	0.037	27.693	28.973
		2	1.120	5,474		0.055	24.954	
		3	0.863	6,803		0.037	34.272	

[1]Variety

TABLE A-7.--Theoretical and experimental values of the critical buckling loads for the lower portion of the plant.

Test Number	Date	Sample Number	Theoretical Value for Theory of Elastic Stability, lb	Type of Buckling from Load Deformation Curve	Experimental Buckling Load, lb
			Comanche[1]		
1st Test	7/7/65	1	1.034	Elastic-Plastic	0.546
		2	2.038	Elastic-Plastic	0.860
		3	1.500	Elastic	0.870
2nd Test	7/14/65	1	0.696	Elastic	0.980
		2	0.371	Elastic-Plastic	0.546
3rd Test	7/21/65	1	0.597	Elastic	0.560
		2	0.438	Elastic	0.540
		3	0.690	Elastic	0.608
4th Test	7/28/65	1	0.887	Elastic and Some Plastic	0.560
		2	1.288	Elastic and Some Plastic	1.190
		3	1.524	Elastic-Plastic	1.700
			Redcoat[1]		
1st Test	7/7/65	1	3.169	Elastic-Plastic	1.054
		2	3.225	Elastic-Plastic	1.056
		3	3.432	Elastic-Plastic	1.058
2nd Test	7/14/65	1	1.099	Elastic-Plastic	1.366
		2	0.967	Elastic-Plastic	0.562
		3	0.680	Elastic-Plastic	0.806
3rd Test	7/21/65	1	1.220	Elastic-Plastic	0.912
		2	0.722	Elastic-Plastic	0.712
		3	1.463	Elastic-Plastic	1.168
4th Test	7/28/65	1	1.263	Elastic	1.028
		2	2.212	Elastic-Plastic	1.674
		3	1.851	Elastic-Plastic	2.200
			Genesee[1]		
1st Test	7/7/65	1	2.365	Elastic-Plastic	1.092
		2	2.384	Elastic-Plastic	1.088
		3	3.293	Elastic-Plastic	1.094
2nd Test	7/14/65	1	2.181	Elastic-Plastic	1.730
		2	2.795	Elastic-Plastic	2.106
		3	1.489	Elastic-Plastic	2.106
3rd Test	7/21/65	1	2.173	Elastic-Plastic	2.380
		2	1.568	Elastic-Plastic	1.012
4th Test	7/28/65	1	2.069	Elastic-Plastic	1.600
		2	1.805	Elastic-Plastic	1.620
		3	2.606	Elastic-Plastic	2.084

[1]Variety

TABLE A-8.--Theoretical and experimental values of the critical buckling loads for the upper portion of the plant.

Test Number	Date	Sample Number	h_o/h_m	μ	Theoretical Buckling Load, lb	Type of Buckling	Experimental Buckling Load, lb
Comanche[1]							
1st Test	7/7/65	1	0.773	0.77889	0.398	Elastic	0.110
		2	0.789	0.79377	0.644	Elastic	0.260
2nd Test	7/14/65	1	0.895	0.89710	0.303	Elastic	0.160
		2	0.863	0.86574	0.297	Elastic	0.166
3rd Test	7/21/65	1	0.800	0.80400	0.267	Elastic	0.120
		2	0.783	0.78819	0.188	Elastic	0.112
		3	0.789	0.79377	0.216	Elastic	0.140
4th Test	7/28/65	1	0.800	0.80400	0.325	Elastic	0.200
		2	0.917	0.91866	0.738	Elastic-Plastic	0.613
		3	0.752	0.75936	0.504	Elastic-Plastic	0.200
Redcoat[1]							
1st Test	7/7/65	1	0.810	0.81380	0.831	Elastic	0.600
		2	0.833	0.83634	0.678	Elastic	0.500
		3	0.836	0.83928	1.133	Plastic	0.800
2nd Test	7/14/65	1	0.783	0.78819	0.448	Elastic-Plastic	0.340
		2	0.842	0.84516	0.244	Elastic	0.156
		3	0.825	0.82850	0.371	Elastic-Plastic	0.240

3rd Test	7/21/65	1	0.857	0.85986	0.563	Elastic	0.446
		2	0.889	0.89122	0.292	Elastic	0.212
		3	0.918	0.91964	0.539	Elastic-Plastic	0.272
4th Test	7/28/65	1	0.800	0.80400	0.400	Elastic	0.228
		2	0.808	0.81184	0.836	Plastic	0.950
		3	0.863	0.86574	0.757	Plastic	1.200
				Genesee[1]			
1st Test	7/7/65	1	0.792	0.79656	0.503	Elastic-Plastic	0.340
		2	0.857	0.85986	0.595	Elastic Plastic	0.374
		3	0.850	0.85300	0.797	Plastic	0.482
2nd Test	7/14/65	1	0.849	0.85202	0.404	Elastic-Plastic	0.254
		2	0.892	0.89416	0.836	Plastic	0.754
		3	0.888	0.89024	0.446	Elastic-Plastic	0.356
3rd Test	7/21/65	1	0.852	0.85496	0.720	Elastic	0.440
		2	0.824	0.82752	0.231	Elastic	0.160
		3	0.916	0.91768	0.456	Elastic-Plastic	0.380
4th Test	7/28/65	1	0.789	0.79377	0.924	Plastic	0.688
		2	0.885	0.88730	0.776	Plastic	0.960
		3	0.944	0.94512	0.917	Plastic	1.000

[1]Variety